STRUCTURAL CHARACTERIZATION OF ATOMICALLY THIN HEXAGONAL BORON NITRIDE VIA RAMAN SPECTROSCOPY

THESIS

J. Matthew Bondy, Captain, USAF

AFIT-ENP-14-M-02

**DEPARTMENT OF THE AIR FORCE
AIR UNIVERSITY**

AIR FORCE INSTITUTE OF TECHNOLOGY

Wright-Patterson Air Force Base, Ohio

AFIT-ENP-14-M-02

STRUCTURAL CHARACTERIZATION OF ATOMICALLY THIN HEXANGONAL
BORON NITRIDE VIA RAMAN SPECTROSCOPY

THESIS

Presented to the Faculty

Department of Engineering Physics

Graduate School of Engineering and Management

Air Force Institute of Technology

Air University

Air Education and Training Command

In Partial Fulfillment of the Requirements for the

Degree of Master of Science

J. Matthew Bondy, BS

Captain, USAF

March 2014

AFIT-ENP-14-M-02

STRUCTURAL CHARACTERIZATION OF ATOMICALLY THIN HEXANGONAL
BORON NITRIDE VIA RAMAN SPECTROSCOPY

J. Matthew Bondy, BS
Captain, USAF

Approved:

_____//signed//_____	_____12MAR14_____
Maj Timothy W.C. Zens, PhD (Chair)	Date
_____//signed//_____	_____13MAR14_____
Yung K. Yeo, PhD (Member)	Date
_____//signed//_____	_____13MAR14_____
Michael R. Snure, PhD (Member)	Date
_____//signed//_____	_____13MAR14_____
Elizabeth A. Moore, PhD (Member)	Date

Abstract

A non-destruction evaluation of atomically thin hexagonal boron nitride (*h*-BN) films is critical to the U.S. Air Force and Department of Defense initiatives pursuing graphene-based electronic field effect transistors (FETs) capable of operating at terahertz frequencies. *H*-BN thin films an increase to the characteristic E_{2g} 1367cm^{-1} *h*-BN peak intensity has been correlated to an increase in film thickness. Raman spectroscopy on a *h*-BN film with thicknesses of 7, 14, and 21 atoms (2.5nm, 5nm, 7.5nm respectively) revealed a linear relationship between peak intensity and thickness. This relationship can mathematically be described as $y = 0.0265x + 0.8084$, and fits the data with a R^2 value of 0.9986. There was no observed correlation between film thickness and full width at half maximum (FWHM) and there was no measured shift to the E_{2g} peak with increasing film thickness.

Acknowledgements

Table of Contents

List of Figures

List of Equations

STRUCTURAL CHARACTERIZATION OF ATOMICALLY THIN HEXAGONAL

BORON NITRIDE VIA RAMAN SPECTROSCOPY

I.   Introduction

1.1   Motivation

The research and development of atomically thin (2D) hexagonal boron nitride (h-BN), leading to the fabrication of next-generation graphene field effect transistors (FETs), is of significant importance to the Air Force and Department of Defense. Such FETs would meet the government's ever present need for smaller, lighter and more energy efficient sensors and structural elements critical to air and space operations. The current state-of-the-art for high-electron-mobility transistor (HEMT) electronics are based on group IV and III-V semiconductors, such as InGaAs and InP, that are not capable of achieving terahertz frequencies due to limited transistor cutoff frequencies well below 1,000 GHz [1]. The proven ability of h-BN to insulate graphene from phonon interaction and preserve it's high electron mobility of 100,000 cm^2/Vs is critical to any eventual device fabrication [2][3]. The coupling of graphene's zero bandgap with h-BN's extremely wide (5.5eV) bandgap provides the opportunity for ultra-fine tuning electromagnetic infrared photodetectors, frequency mixers, and analog-to-digital (A/D) converters [4][5].

An in-depth non-destructive structural characterization of atomically thin hexagonal boron nitride is of particular importance in trying to develop a dielectric substrate material that compliments the high mobility zero-bandgap semiconducting

properties found in graphene [5]. Given that graphene is a 2D material aligned in a

hexagonal lattice it follows that a desired substrate would have a similar 2D structure; *h*-

BN is such a material. With a small 1.7% lattice mismatch when compared to graphene,

h-BN is well-suited as a substrate and potentially for eventual device fabrication. The

hybridization of *h*-BN/graphene heterostructures would allow for a finely tuneable

bandgap to be designed directly into a system as needed [6]. The Sensors Directorate of

the United States Air Force Research Laboratory (AFRL/RY) is currently conducting

research into the fabrication and implementation of *h*-BN/graphene films for device

fabrication and utilization in silicon integrated circuits (ICs). One of the greatest

contributions of *h*-BN/graphene electronic structures would be the ability to "tune"

graphene's zero-bandgap from 0-0.4 eV within the previously unattainable terahertz

frequencies through the application of an electric field. This breakthrough into

operational terahertz ranges would yield far-reaching applications ranging from non-

destructive defect detection in mechanical structures, advanced spectroscopy resolution,

and ultra-high capacity communication links to sub-MMW radar systems. Hexagonal

boron nitride is a well studied material and has been a widely pursued area of research

with demonstrated value as an ultra-high temperature industrial lubricant and protective

coating additive, as a deep ultraviolet (DUV) emitter, and used as a dielectric for

nanoelectronics [7]. Furthermore, amorphous boron nitride films have also successfully

been doped with carbon for use in neutron detectors [8].
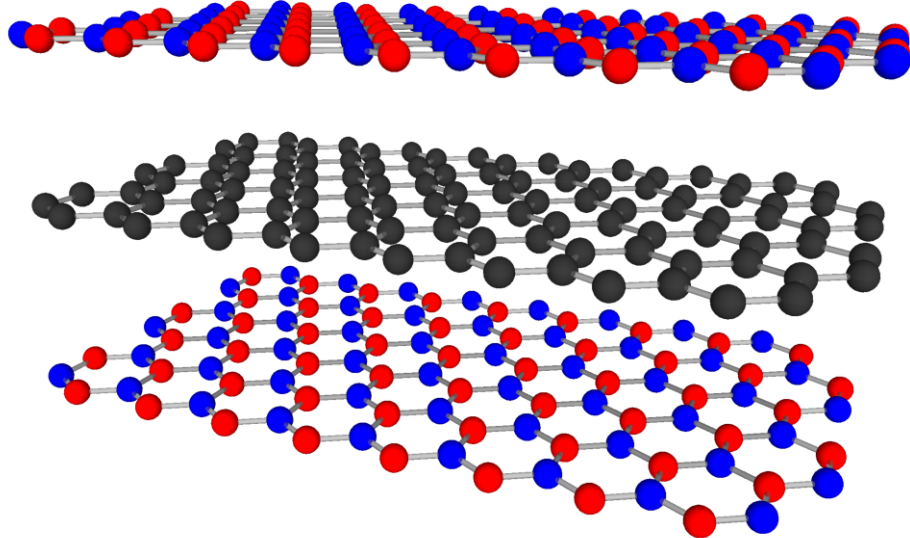
Figure 1.1: Currently, only graphene on a *h*-BN substrate has been shown to preserve graphene's mobility of 100,000 cm^2/Vs [9]. The two lattices have only a 1.7% mismatch and complimentary hexagonal planar structures with weak inter-planar bonding allows *h*-BN to insulate graphene from thermal phonon interactions which would otherwise cause electron scattering and degradation of graphene's high electron mobility.

Comparable materials being pursued would be InSb or InGaAs with cutoff frequencies above 100 GHz and 400 GHz [10], respectively, and room temperature channel mobilities of ~10,000 cm^2/Vs and ~3,000 cm^2/Vs [11], respectively. Given the high atomic number of indium and antimony the interatomic bonding is relatively weak and limits the amount of voltage the system is able to maintain. It has been shown by Britnell *et. al.* that the selection of *h*-BN/graphene hetero-structures as a re-engineered approach to high-electron mobility transistors would outperform the theoretical 10^3 switching ratio of current state-of-the-art silicon-based electronic InP and GaAs HEMTs by approximately an order magnitude (see Figure 1.2) [12].
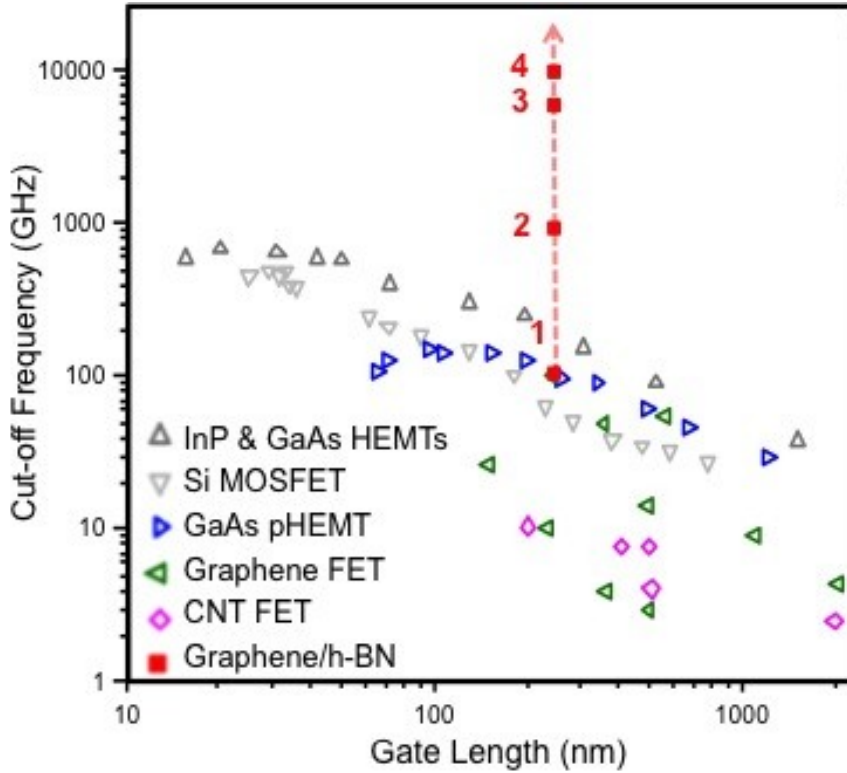
Figure 1.2: Chart of current field-effect transistors performance parameters as a function of cut-off frequency and gate length [1] (1) Record graphene FET with μ=1500 cm^2/Vs (2) Graphene on SiC μ =10,000 cm^2/Vs (3) Graphene on *h*-BN μ =40,000 cm^2/Vs reported by Dean *et. al.* in 2010 [2] (4) Graphene on *h*-BN μ =100,000 cm^2/Vs as reported by Mayorov *et. al.* in 2011 (Data from Britnell *et. al.* [12]).

The primarily pursued application of *h*-BN/graphene hetero-structures is as FETs for use in terahertz technology switching applications. DARPA's initiation of the THz electronics program in July 2012 further emphasizes the DoD and the government requirement to operate within the terahertz range [13]. The use of *h*-BN instead of traditional SiO$_2$ provides an alternative gate dielectric while maintaining nearly no loss of graphene's key performance parameters. Both the wide bandgap and high polarizability of *h*-BN characterize it as prime dielectric material.

4

Conducting a thorough investigation of *h*-BN's shear mode via Raman spectroscopy will yield useful insight into defects, stacking sequence, and thickness characteristics for utilization in the fabrication of *h*-BN/graphene hetero-structures. Non-destructive analysis of laboratory produced *h*-BN films will provide critical process improvement feedback necessary to refine atomically thin fabrication techniques. Current characterization techniques commonly used to determine thickness, stacking sequence, and defect concentration in *h*-BN include transmission electron microscopy (TEM) and atomic force microscopy (AFM) both of which often cause damage to monolayer *h*-BN thereby rendering the sample unusable as a graphene substrate. TEM exploits the small de Broglie wavelength of electrons to image materials by passing a beam of electrons through a thin film of material. Such high powered electrons can damage the lattice of any atomically thin *h*-BN that is to be investigated. Similarly, the AFM utilizes an atomically sharp needle point mounted at the end of small mechanical arm that is brought close to a material's surface. By analyzing the resulting frequency of the cantilevered tip vibrations, brought about by electric potentials experienced between the tip and material's surface, one can gain a sub-nanometer resolution image of a material. AFM is not well suited to investigating atomically thin *h*-BN due to it's inability to perform material identification and the high likelihood of the AFM tip to snag and damage the examined films.

1.2   Research Topic

Boron nitride is a widely investigated group III-V material with particular focus given to *h*-BN's unique anisotropic characteristics [14][15]. Boron nitride is a wide band gap material possessing a direct band gap of 5.971 eV, greater than the 5.5 eV band gap
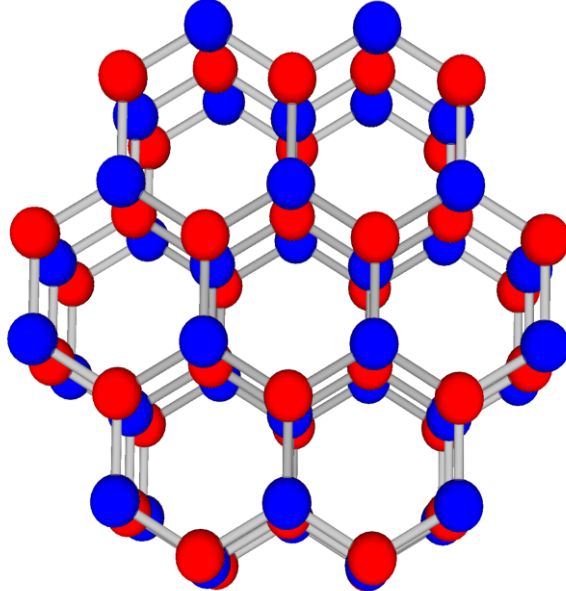
Figure 1.3: Schematic of *h*-BN AA' Bernal stacking sequence of alternating boron atoms (red) and nitrogen atoms (blue)[36]. Both graphene and *h*-BN arrange in large sheets of honeycomb formations with strong in-plane bonding and weak interplanar bonding. The close lattice spacing of *h*-BN to graphene with (a_{BN}=0.250 nm and a_c=0.246 nm; c_{BN}=0.666 nm and c_c=0.674 nm) suggests that the two materials would stack well together [37].

of diamond [4][16]. Boron nitride commonly forms hexagonal and cubic crystal structures which are often considered analogous to carbon in its graphite phase and diamond phase, respectively. In it's hexagonal crystalline structure boron nitride forms large planar sheets of covalently bonded boron and nitrogen atoms with a 1:1 ratio in either a AA'A or ABA Bernal stacking structure [4][17][18]. This planar structure

results in weak interlayer forces bonded via columbic attraction or Van der Waals forces. Owing to these weak interlayer bonds *h*-BN is widely used as a lubricant in industrial applications requiring stability over large temperature ranges and under oxidizing conditions [7].

1.3 Graphene and *h*-BN/Graphene Hetero-structures

The discovery of free standing graphene in 2004 ushered in the next generation of materials that may one day make room temperature THz electronic performance a reality. Graphene possesses massless Dirac fermions with a carrier concentration mobility at room temperature of 100,000 cm^2/Vs, higher than any known material [5]. This mobility combined with high transconductance and low access resistance make graphene an ideal candidate for ultra high-speed analog applications. Given graphene's high carrier mobility it is well suited for integrated circuit applications such as being used as the channel in a field-effect transistor.

Ultra high-speed electronic switching has garnered widespread attention with IBM's announcement in December 2008 that they had successfully fabricated graphene transistors operating in the GHz range [19] and with DARPA's initiation of a HEMT research program [13]. Graphene's high mobility and other electrical properties are currently only achievable in a vacuum due to substrate phonon interactions with the graphene that act to greatly degrade its inherent properties, and thus hindering translation to real-world applications. Pairing graphene with a substrate that preserves its electrical characteristics while effectively shielding it from external influences is critical to the advancement of next-generation electronic devices [6]. The hybridization of *h*-BN and

graphene could also lead to the development of "layered sensing" capabilities to include transparent electronics fused within a device's aperture.

1.4   Research Scope

This study focuses solely on the characterization of atomically thin hexagonal boron nitride (produced by AFRL/RY) utilizing Raman spectroscopy to investigate key attributes such as film thickness, defect concentration, and lattice structure. This research marks the beginning of a greater effort to develop a process for the fabrication of atomically precise *h*-BN films for the development of new innovative wafer-scale *h*-BN/graphene electronic devices on semiconducting substrates capable of operating in the THz range.

Unlike graphene, *h*-BN is not easily distinguished due to its high optical transparency and the lack of a characteristic Raman shift in the G' peak. In order to properly understand and accurately count the number of *h*-BN/graphene layers synthesized, it is necessary to develop a methodology to measure *h*-BN thickness via Raman spectroscopy. This technique can then be used when analyzing *h*-BN/graphene hetero-structures.

1.5 Document Structure

This document is divided into five chapters: (1) Introduction, (2) Background and Theory, (3) Experimental Procedure and Equipment, (4) Results and Analysis, and (5) Conclusion. Chapter 1 of this thesis is the Introduction which details the relevance and motivation of investigating atomically thin *h*-BN in support of Air Force and DoD initiatives. The Introduction also includes an overview of boron nitride, the use of

potential h-BN/graphene heterostructures, as well as codifying the scope of research that this project sought to encapsulate. Chapter 2, Background and Theory, provides the reader with a top-level overview of Raman spectroscopy, optical and electronic properties of two-dimensional materials, and the role of Raman spectroscopy in investigating those two-dimensional materials. Furthermore, Chapter 2 discusses possible h-BN/graphene device applications as well as the structure, binding, Raman active modes, and fabrication of atomically thin h-BN films. Chapter 3, Experimental Procedure and Equipment, documents unique obstacles to the characterization of two-dimensional materials, low wavenumber Raman Analysis of h-BN, possible correlation of a shift of the E_{2g} 1367 cm^{-1} h-BN peak to film thickness and the use of depth profiling to maximize spectral returns. Chapter 3 also outlines the experimental set-up and procedures related to collecting the h-BN spectra to include the selection of appropriate excitation sources, use of filtering packages, and focusing objective. Chapter 4, Results and Analysis, details the spectral returns of two unique h-BN sites of the same sample which had undergone tearing/folding during the fabrication process allowing for investigation of incremental increases in film thickness via Raman spectroscopy and Atomic Force Microscopy (AFM). Chapter 4 presents AFM thickness results which are then compared to the two sets of h-BN computer-analyzed Raman spectral returns. Chapter 5, Conclusion and Future Research, provides an executive summation of the findings of this thesis as well as recommendations for future research.

II. Background and Theory

This chapter details the background of two-dimensional materials with regards to both their optical and electronic characteristics as well as a brief overview of Raman spectroscopy theory as related to two-dimensional materials. Furthermore, this chapter discusses the material properties of boron nitride, with an emphasis on the hexagonal phase, along with potential applications of atomically thin *h*-BN films both as a standalone system a well as when coupled with graphene.

2.1 Raman Spectroscopy

2.1.1 Raman Spectroscopy Overview

Raman spectroscopy provides a valuable method to non-destructively analyze a material's composition and atomic structure through the analysis of an incident photon shift induced by phonon coupling. Raman spectroscopy is an optical phenomenon and can be utilized to investigate a material in any of its phases (i.e. gas, liquid, solid) and provide detailed insight into molecular rotational and vibrational modes [20]. Spectra gathered via Raman spectroscopy can yield insight into a material's solid phase, analysis of vibrational modes can dictate long and short crystalline order, grain size, presence of surface contaminants, crystal orientation, and overall material quality.

A basic understanding of Raman spectroscopy lies in Raman scattering, a phenomenon named after Sir Chandrasekhara V. Raman who experimentally observed in 1928 (and was subsequently awarded the 1930 Nobel Prize in Physics) that a small fraction of photons deviated from the expected Rayleigh scattering pattern which had

been theorized by Adolf Smekal in 1923 [21][22]. Raman scattering occurs from the inelastic scattering of monochromatic photons due to interaction with a material's phonons. Figure 2.1 illustrates this interaction as contrasted with both Rayleigh scattering and infrared absorption.
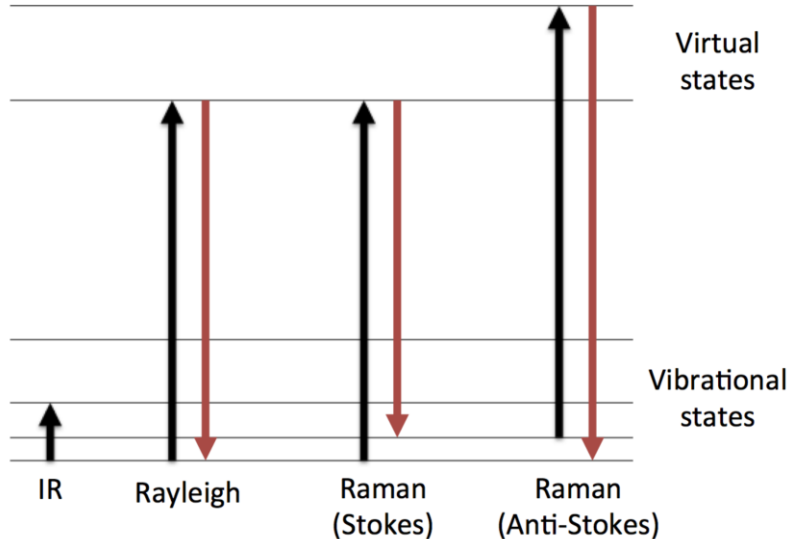
Figure 2.1: Diagram depicting both anti-Stokes and Stokes Raman scattering as compared to Rayleigh scattering and Infrared absorption. Note that the majority of reflected photons, when incident on a surface, return at their original wavelength because these photons interact elastically with the sample material. However, every 1:1,000,000 photons incident on a surface will interact inelastically with the material due to phonon-coupling and will be scattering at either a higher frequency (anti-Stokes) or at a lower frequency (Stokes). Through the analysis of this shift a great deal of information concerning a material's rotational and vibrational modes can be understood.

Raman scattering occurs when a photon is incident on a material and inelastically "collides" (or couples) with a phonon causing the photon to either be excited into a higher (or lower energy) state thereby resulting in a shift from the original frequency of the photon. Because the phonon acted upon will return to its original state through the emission of a frequency-shifted photon (scattered from the original laser line) this

excitation is said to be to a "virtual" state. A photon is said to undergo anti-Stokes Raman scattering if the scattered photon is of higher energy than the original photon (i.e. blue-shifted). Similarly, a photon undergoes Stokes Raman scattering if the scattered photon is of lower energy than the original photon (i.e. red-shifted). It should be noted that Raman scattering is an extremely weak phenomenon only occurring in approximately 1 in a million incident photons [23].

2.1.2 Raman Spectroscopy Theory

Similar to Rayleigh scattering, Raman scattering has a direct dependence on the polarizability of a molecule. Molecules that undergo polarization from an incident photon can cause the inelastic scattering of that photon, thereby shifting or "scattering" that photon's wavelength to a greater or diminished energy state as shown in Figure 2.1. A diatomic molecule such as boron nitride is both Raman active and IR active due to is heteronuclear structure. Changes to the bond length and molecular bending serve to change both the polarizability (necessary for a Raman signature) and the dipole moment of the molecule (necessary for an IR signature). This dual Raman and IR activity allows for the independent IR signature verification that boron nitride has been deposited on a surface where there may be no optical indicators to help guide a Raman return.

By exciting vibrational modes within a molecule an incident photon can impart energy to the material via a phonon-coupling interaction and be scattered back at a lower energy wavelength than the Rayleigh line, this lowered energy state is referred to as "Stokes" scattering. Conversely, occasionally the investigated material may impart energy to an incident photon causing it to scatter at a higher energy level than the

Rayleigh line, this heightened energy state is referred to "anti-Stokes" scattering. While both Stokes and anti-Stokes Raman scattering are an extremely rare phenomenon occurring on the order of one in a million to incident photons, the anti-Stokes or imparting of energy to a scattered photon is more rare than Stokes scattering. Because both anti-Stokes and Stokes scattering are mirror compliments of one another, it is often the practice of Raman spectroscopy to filter out both the Rayleigh laser line and anti-Stokes lines to solely isolate the Stokes lines for analysis.

Equation 1, the fundamental Raman equation, describes the inelastic scattering undergone by a photon incident upon a molecule,

$$\hbar\nu + E_i = \hbar\nu' + E_f \tag{1}$$

where ν is the frequency of the incident photon, E_i is the initial energy state of the molecule, ν' is the scattered photon frequency, $\hbar$ is Planck's constant, and E_f is the final energy state of the molecule [24]. If $\nu > \nu'$ than the incident photon is of a lesser energy than the scattered photon resulting in an anti-Stokes transition. Similarly, if $\nu < \nu'$ than the scattered photon is of a lesser energy than the incident photon resulting in Stokes transition.

A set of selection rules exist for polyatomic molecules to determine whether a molecule is Raman active (able to inelastically interact with an incident photon). Given that the quantum numbers of all other molecular modes remain the same, only a single mode must change in order to bring about a Raman transition. The quantum number v_i must change by a non-zero integer step for a Raman transition to occur, for example

$$\Delta v_i = \pm 1 \tag{2}$$

$$\Delta v_j = 0 \; for \; j \neq i,$$

where v_i denotes the quantum number of the i [th] vibrational mode of the polyatomic

molecule.

Rearranging Equation 1, an expression for the Raman frequency shift Δv can be

developed relative to the incident frequency,

$$\hbar(v' - v) = E_i - E_f.$$

Substituting $\Delta v = (v' - v)$ and dividing by $\hbar$ yields

$$\Delta v = (v' - v) = \frac{E_i - E_f}{\hbar}$$

Applying Equation 2 the transition from $v_i'' \rightarrow v_i'$ is given by

$$\Delta v = v_{0i}(v_i'' - v_i') = \mp v_{0i}, \tag{3}$$

where v_{0i} represents the harmonic vibrational frequency in the molecule of the i [th]

vibrational mode. Equation 3 indicates that a Raman active polyatomic molecule will

inelastically scatter light at known frequencies. These frequencies not only allow for

material identification but also allow for insight into a material's atomic structure given

that certain frequencies will only occur from particular structural configurations. The

number of Raman frequencies present in a material is directly related to the vibrational

degrees of freedom (DOF) present in that system,

Linear: $\qquad\qquad DOF = 3N - 5$ \hfill (4)

Nonlinear: $\qquad\qquad DOF = 3N - 6.$ \hfill (5)

With regard to Equation 4, the subtraction of five accounts for the presence of

three translational degrees of freedom and two rotational degrees of freedom. Nonlinear

molecules experience a third rotational degree of freedom leading to the subtraction of six (instead of five) in Equation 5.

2.2 Atomic Force Microscopy

Chapter IV relies upon independent h-BN film thicknesses acquired via Atomic Force Microscopy (AFM). While extremely useful for thickness measurements AFM has a number of drawbacks, the primary of which for this thesis was the possibility of the AFM tip to damage the delicate h-BN films during the course of a thickness measurement. Originally invented in 1986 by Gerd Binnig and Heinrich Rohrer, for which they won the Nobel Prize in Physics, the AFM utilizes a cantilevered beam equipped with a sharp tip (often only atoms thick at the point) which is brought close to a material's surface to study the effect of the atomic forces experienced by the cantilevered tip. Such atomic forces present at the material's surface may include van der Waals force, capillary, chemical bonding, electrostatic, and magnetic among others. Any resulting vibrations or deflections on the cantilevered beam are measured by either a laser reflected off the beam or through the use of piezoresistive elements within the beam that act as an internal strain gauge.

The AFM can be utilized in three different imaging modes to include a contact, tapping, or non-contact mode. In contact (or static) mode the tip is dragged along the material's surface to directly measure any surface features. Contact mode is rarely used in actual practice given the high likelihood of damaging both the tip and the material being investigated. Tapping (or AC) mode circumvents the common phenomenon of a liquid meniscus layer to form upon a material's surface under normal ambient conditions.

This thin meniscus layer prevents the AFM tip from being brought close enough to the surface to experience short-range forces without becoming "stuck" on the surface. In tapping mode, the AFM tip is vibrated at its resonant frequency and brought close to the surface (without touching the meniscus layer) and any atomic forces present are measured by the deviation from the AFM tip's resonant frequency. In non-contact mode, the AFM tip is once again caused to oscillate at or near its resonant frequency, however, the utilization of a feedback loop counteracts any forces exerted on the tip to maintain a constant frequency. By measuring the required resistance to maintain this constant frequency a material's surface topography can be extrapolated.

For the purposes of this thesis, the AFM was used solely as a source of independent thickness validation from which to correlate any subsequent Raman analysis. Routine use of the AFM for thickness measurements is not desirable because the AFM tip could snag the h-BN film edge or otherwise damage the film. AFM is also limited in its scope, it is primarily used for surface topography and is not readily used for material identification or characterization, both of which are vital to the investigation of atomically thin h-BN.

2.3 Optical & Electronic Properties of 2D Materials

With the discovery of free standing two-dimensional graphene in 2010 the scientific community has gravitated towards the exploration of an entirely novel class of two dimensional materials. What began with graphene has spread to the fabrication and analysis of numerous two-dimensional materials to include monolayer molybdenum disulfide, silicene, germanane, h-BN, and black phosphorous [25].

Traditionally, when conducting an optical analysis of a material neutron scattering is the preferred method to gain insight into the behavior of a material's various optical modes. However, due to the necessity finding an available neutron source, a nuclear reactor is the most commonly used source, a less resource intensive approach must be cultivated. For this reason, Raman spectroscopy is an ideal candidate to identify the optical modes present in atomically thin h-BN films.

The electronic properties of 2D materials vary from bulk materials due to a lack of multiple layer interactions. This difference becomes very prominent in 2D materials despite their typically weak (and often negligible) influence on system behavior. For instance, graphene is a zero-gap semiconductor due to its electronic structure while graphite is a semimetal with a band overlap [1].

Previously noted in Chapter 1 and Figure 1.2, current device improvements through the reduction of FET gate-lengths has reached a theoretical limit due to the transition of material properties from the macro to the micro [1]. At the current industry edge of a 10 nm gate length the bulk properties of silicon greatly deteriorate as atomic phenomenon such as quantum confinement and atomic bond strength breaking impede electron mobility. Two-dimensional materials, such as graphene with a carrier mobility of 100,000 cm^2/Vs [5], provide a solution surpassing the theoretical limit of silicon and to achieving higher FET electron throughput without introducing the adverse material properties of sub-10 nm gate lengths.

2.4 Overview of Raman Spectroscopy of 2D Materials

Recent advancements in photon detection device sensitivity as well as precision filtering packages allows for the exploration of materials via Raman spectroscopy that historically would have been prohibitive. Noted by Beghi *et al.* thin films tend to experience a large substrate return indicative of the transparent nature of most atomically thin films, this is particularly true of *h*-BN [26]. As will be discussed in the next chapter, precision mechanical elevation control greatly enhanced the investigation of *h*-BN thin films through systematic depth profiling of a sample to maximize the Raman spectral return from the 2D film. Depth profiling takes advantage of the conical shape of the focused laser beam to preferentially sample the desired *h*-BN thin film while reducing an otherwise overwhelming substrate return. As detailed by the Manchester Centre for Mesoscience & Nanotechnology there exists a potential correlation between an upshift of the characteristic 1367 cm^{-1} *h*-BN peak and film thickness which should allow for distinguishing between layers utilizing a combination of optical contrast and scanning probe methods[27].

2.5 Hexagonal Boron Nitride

The various polytypes of boron nitride are often seen as analogous to the various forms of carbon. The sp^2 bonded hexagonal boron nitride and sp^3 bonded cubic boron nitride are comparable to graphite and diamond, respectively [28]. In 2006 Arnaud *et. al.* *h*-BN is described as "one of the most anisotropic layer compounds and represents an interesting quasi-two-dimensional insulator analog to semimetallic graphite" [29]. The

pursuit of research based upon *h*-BN/graphene device applications can be seen as a natural outgrowth of these similarities between boron nitride and carbon (i.e. graphene).

2.5.1 Structure

Boron nitride commonly occurs in either hexagonal or cubic structures with a less common wurtzite structure having been achieved via laboratory fabrication [30]. Given that boron nitride is a purely synthesized material through the use of boric acid or boron trioxide and not found in nature it's atomic structure is subject to carefully controlled laboratory conditions. This regimented approach to fabrication has allowed the continued refinement to the purity and quality of synthesized boron nitride and has led recently to the first single walled boron nitride nanotubes (SW-BNNT) being produced [31]. The hexagonal configuration of boron nitride (*h*-BN) forms purely interplanar bonds resulting in large sheets of single atom thicknesses, analogous to graphene. Because there are no out-of-plane bonds, *h*-BN easily slides along other atomic sheets of *h*-BN lending it to applications as a high heat industrial grade lubricant. The lack of out-of-plane bonds also allows for the formation of boron nitride nanotubes, which are analogous to carbon nanotubes (CNT). BNNTs can be doped with gold particles to form FETs or can be doped with europium to create phosphor visible light emitters when stimulated by electrons.

2.5.2 Raman Active Modes

In 1966 Geick *et. al.* published a detailed theoretical examination of *h*-BN demonstrating it to have 4 Raman active optical modes resulting in two single Raman lines once polarization is considered [14]. Due to the high symmetry of *h*-BN the two in-plane modes and the two shear modes occur at the same Raman shift and have an additive effect resulting in one in-plane mode and one shear mode. These two *h*-BN Raman active modes occur as either a high-energy phonon (in-plane mode) at a Raman shift of 1367 cm^{-1} [15] [28] or as a low frequency phonon (shear mode) at 52.5 cm^{-1} [28].
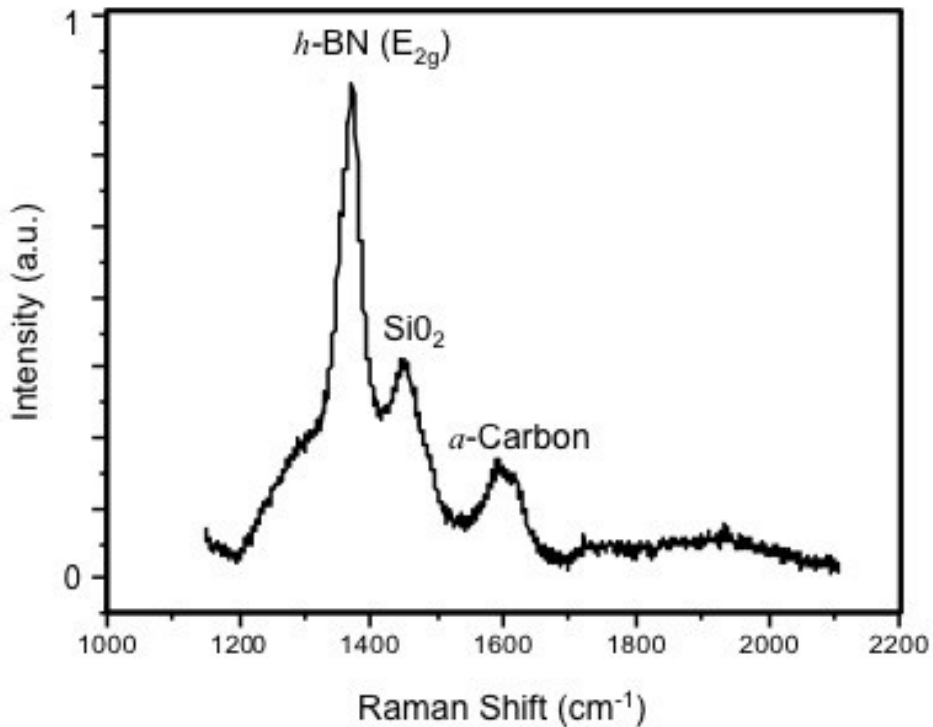
Figure 2.2: Raman spectra of *h*-BN with the 1367 cm^{-1} E$_{2g}$ peak labeled [15].   A lower intensity and broader peak around ~1600 cm^{-1} was attributed to the G and D' peaks of carbon introduced to the system through the transfer process via thermal release tape [35]. The 1448 cm^{-1} peak is attributed to a higher order SiO$_2$ combination peak given that it also appears in Raman analysis of pure SiO$_2$ wafers.

20

The presence of a high and low frequency mode is to be expected given that atomically thin h-BN forms strong interplanar ionic bonds between the nitrogen and boron atoms (high frequency mode), with only Van der Waals force binding between separate layers (low frequency mode). The Raman active high energy phonon at 1367 cm^{-1} is an irreducible $E_{2g(2)}$ representation of the D_{6h} point group and is caused by intralayer vibrations and the $E_{2g(1)}$ (52.5 cm^{-1}) phonon mode is attributed to shearing from rigid layer vibrations.

2.6 Overview of h-BN Film Fabrication & Sample Preparation

The atomically thin h-BN films utilized for this study were grown by AFRL/RY via metal oxide chemical vapor deposition (MOCVD) in a cold-walled reactor at 900 °C on a copper catalyst. Trimethyl bromide and ammonia were used as precursors with a hydrogen flow motivator across a Cu-foil catalyst heated to 900 °C via a pyrolytic boron-graphite heater. The Cu-foil is a necessary catalyst to reduce the growth temperature of h-BN from 1500 °C to 900°C to achieve greater crystalline structure and uniformity. To transfer the h-BN from the copper catalyst to the 300 nm SiO_2/Si substrate for analysis a 1 molar solution of iron trichloride was used to dissolve the copper. The film was then rinsed with de-ionized water (H_2O) and transferred to the SiO_2/Si substrate via thermal release tape which was subsequently heated to 80 °C to deposit the h-BN film.

2.7 Summary

This chapter detailed the background of two-dimensional materials with regards to both their optical and electronic characteristics as well as a brief overview of Raman spectroscopy theory as related to two-dimensional materials with an emphasis on h-BN

and the growth MOCVD method utilized for producing atomically thin *h*-BN. Key characteristics of *h*-BN include it's 1.7% optical contrast (i.e. transparent to the naked eye) and it's wide bandgap of 5.971 eV [4] (greater than diamond). Furthermore, this chapter discusses the material properties of boron nitride, with an emphasis on the hexagonal phase, along with potential applications of atomically thin *h*-BN films.

III. Experimental Procedure and Equipment

3.1 Characterization Obstacles Unique to BN 2D Films

Due to the difference in scale of *h*-BN films (1-10 atoms thick) to the substrate on which they are grown (~mm) obtaining Raman spectra of atomically thin *h*-BN film presents a unique set of challenges. Despite great advances in laser technology, the ability to focus a coherent laser beam to much less than a micron spot size (at sufficiently high intensities to return a Raman signal) still remains difficult. Because the volume of laser light incident on a given *h*-BN sample is, by it's very nature, thicker than the atomically thin film being analyzed it impossible not to return a Raman spectra of the substrate. Often times, the substrate returns Raman peaks too close to *h*-BN's 1367-peak to resolve any discernable change to the *h*-BN peak. High optical transparency coupled with the mono-layer thickness of most sampled films required longer laser scan times than traditional materials specifically focused at a particular depth above or below the film's surface.

Another obstacle facing the investigation of *h*-BN thin films lays in an the mismatched indices of refraction between the SiO_2 substrate (1.46) and the *h*-BN film (2.1) [32][28]. This index mismatching results in the majority of the light being reflected due to the SiO_2 rather than the *h*-BN resulting in a much stronger substrate signature. The Schlick's approximation of the classic Fresnel equation, shown below, describes this phenomenon of light passing through mediums of differing indices of refraction.

$$R_0 = \frac{(n_{SiO_2} - n_{BN})^2}{(n_{SiO_2} + n_{BN})^2} \tag{6}$$

Solving Equation 6 for the reflective coefficient of *h*-BN yields 3.2%. This means that 96.8% of the light returned from the sample surface is due to SiO_2 reflection rather than desired *h*-BN reflection. To put the challenge of having such a low R_0 into perspective, the reflective coefficient of a glass and air interface is generally taken as 4% meaning that *h*-BN is less reflective than a window.

3.2 Low Wavenumber Raman Analysis

Use of the Near-Excitation Tuneable filter (NExT) allows for Raman returns much closer to the laser line than typically utilized (~5-10 wavenumbers from the laser line). Low wavenumber analysis is important for low energy Raman transitions that occur extremely close to the laser line. As discussed previously, it is experimentally unrealistic to filter out the Raman peaks of the substrate without adversely effecting the BN signal. A possible solution to this obstacle is to investigate the shear mode peak of *h*-BN located at approximately 52.5 cm^{-1} [33] utilizing the NExT filter. Analysis of Raman spectra at these lower wavenumbers supplies an understanding of shear modes which are particularly important in determining stacking sequence and film thickness. The 52.5 cm^{-1} shear mode is produced by interlayer vibrations between *h*-BN mono-layers as opposed to B-N in-plane atomic vibrations which produce the 1367 cm^{-1} characteristic *h*-BN peak. Therefore, one would not expect to see the shear mode peak when investigating a single mono-layer because there would not be another requisite layer to produce an interlayer vibration. However, if the 52.5 cm^{-1} shear mode peak could be examined as a function of film thickness it would be expected to increase incrementally with an increase to film thickness.

3.3 Correlation of Peak Shift to Layer Thickness

In 2011, Gorbachev's *et. al.* paper "Hunting for Monolayer Boron Nitride: Optical and Raman Signatures" presents a possible correlation between a shift in the 1367 cm^{-1} *h*-BN E$_{2g}$ peak with layer thickness. Gorbachev demonstrated an upshift of the 1367 cm^{-1} peak by as much as 4 cm^{-1} allowing for the counting of atomic layers of *h*-BN by exploiting the interger-step increase of both the Raman intensity and optical contrast [27]. A key motivation of this thesis was to examine these results as a possible non-destructive method to ascertaining the structural characteristics of *h*-BN films grown by AFRL/RY. It should be noted that no such shift to the E$_{2g}$ peak was observed in a similar study, "Toward the Controlled Synthesis of Hexagonal Boron Nitride Films" conducted by Ismach *et. al.* in 2012 at the University of Texas at Austin [7].

3.4 Depth Profile Analysis

In order to maximize the Raman signature of the *h*-BN film it was necessary to conduct a depth profile analysis of the sample before collecting a longer dwell-time Raman scan. Figure 3.1 (seen on the next page) demonstrates how the relative volume of material with which the laser light interacts changes as a function of depth. Given that the optical focusing of the laser line creates a conical shape to the laser beam, and that the penetration of the laser light into the sample is constant based on beam power, a greater amount of *h*-BN surface film can be sampled by focusing the beam either above or below the sample surface.
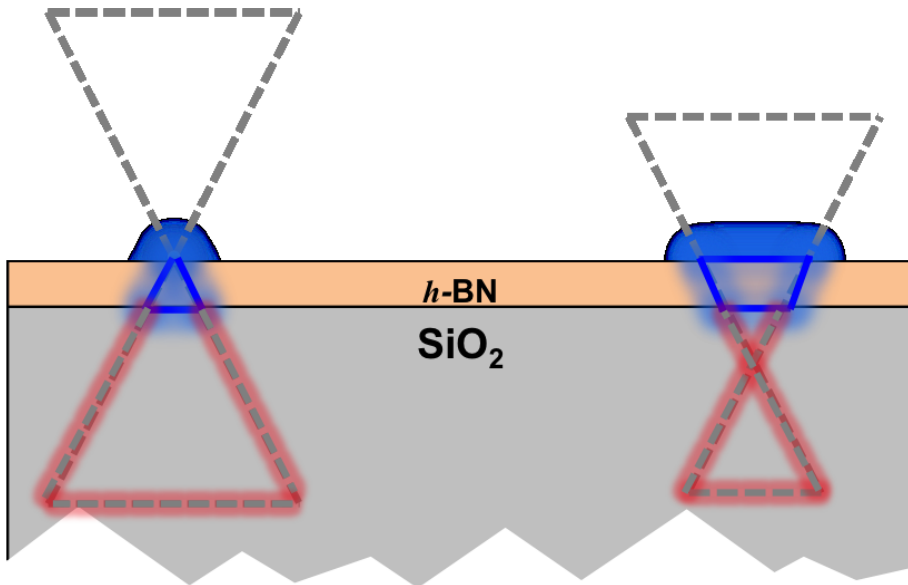
Figure 3.1: Cartoon depicting the relative volume of material sampled by a conically focused laser beam. Note that when focused at a material's surface a larger volume of substrate is sampled versus focusing the laser beam below the surface allowing for a greater film volume to be sample yielding optimal Raman returns.

Boron nitride is a naturally weak Raman scatter. Given this and the thin volume to be sampled it is difficult to get a Raman signature for 2D h-BN. In order to produce the spectra with the best return, a depth profile was performed to locate the depth which produced the highest intensity. This was often not focusing on the surface. Changing the focus increased the laser spot size and thus the sampling volume. The effect on the depth of the focused laser beam on spectral returns can be seen in Figure 3.2. Note that the characteristic E_{2g} h-BN is actually most pronounced at -0.4µm below that sample surface where the conical nature of the beam disproportionately over-samples the thinner h-BN film and under-samples the thicker SiO_2 substrate.
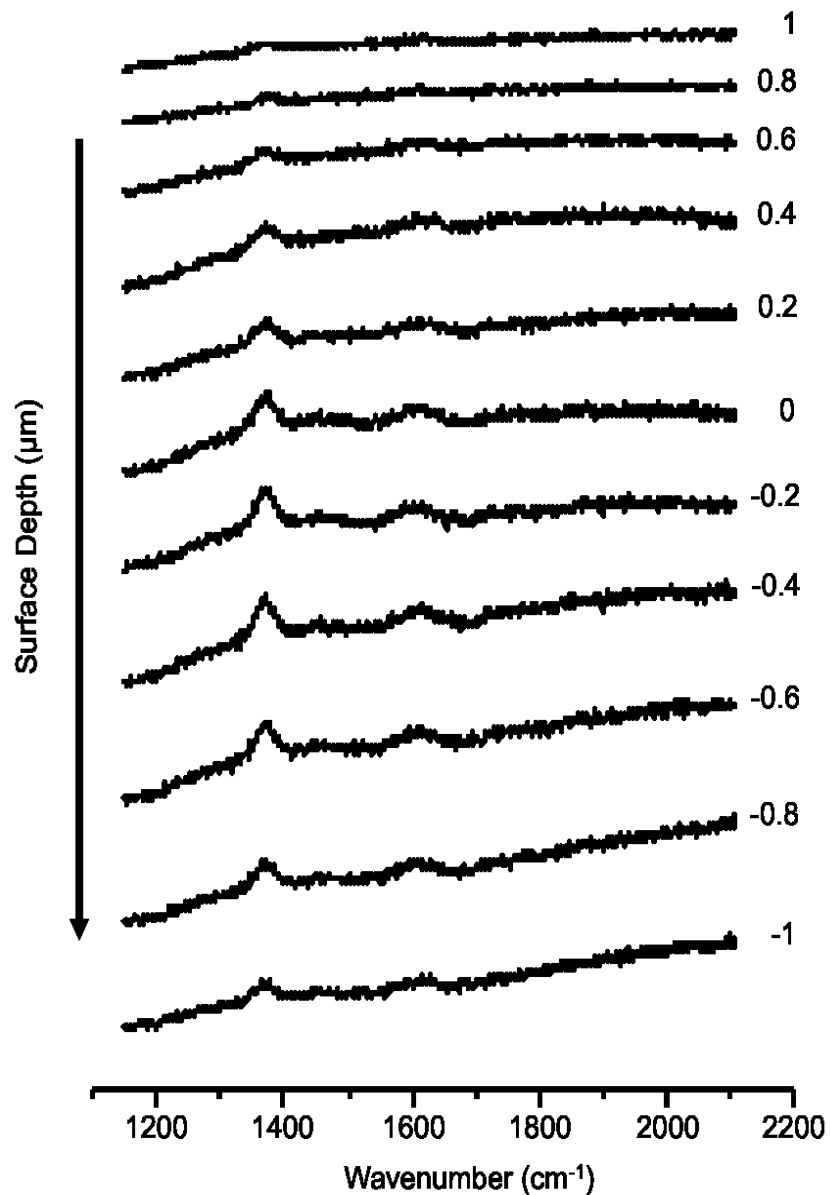
Figure 3.2: Note that the most pronounced *h*-BN 1367cm^{-1} occurs at -0.4μm (z-depth) substantiating the ability to utilize the conical nature of the laser beam to preferentially sample thin films.

3.5 Instrumentation

Modern Raman spectroscopy utilizes five main components to include an excitation source, focusing lens or microscope, a Rayleigh long-pass filter, spectrometer, and detector. As detailed in Figure 3.3 the ability to successfully sample atomically thin *h*-BN relies almost exclusively on the careful consideration of how the Raman spectrometer setup is configured. Maximizing the weak *h*-BN signature over the strong substrate signature is of paramount concern. The use of depth profiling has already been discussed to help maximize the *h*-BN signal, the use of instrumentation configuration will be explored in the subsequent sections.

The Sensor's Directorate Raman Spectroscopy laboratory at the United States Research Laboratory (AFRL/RY) currently maintains the use of two inVia Reinishaw systems with proprietary Reinishaw Wire 4.0 software to control system parameters. Both systems were supported on floating air actuated vibration reduction optical tables to ensure consistent laser output and sample integrity during experimentation. This controlled environment was particularly critical to the longer multi-hour accumulative Raman scans.

3.5.1 Excitation Source

Along with the two inVia Reinishaw Raman microscopes AFRL/RY operates 4 lasers to include an argon ion source capable of 488 nm and 514.5 nm wavelengths, a 532 nm diode source, a helium neon capable of 633 nm, a 785 nm diode source, and a helium cadmium source emitting at 325 nm (see Figure 3.3 below). All lasers were mounted to air actuated floating tables to reduce effects due to ambient vibrations.
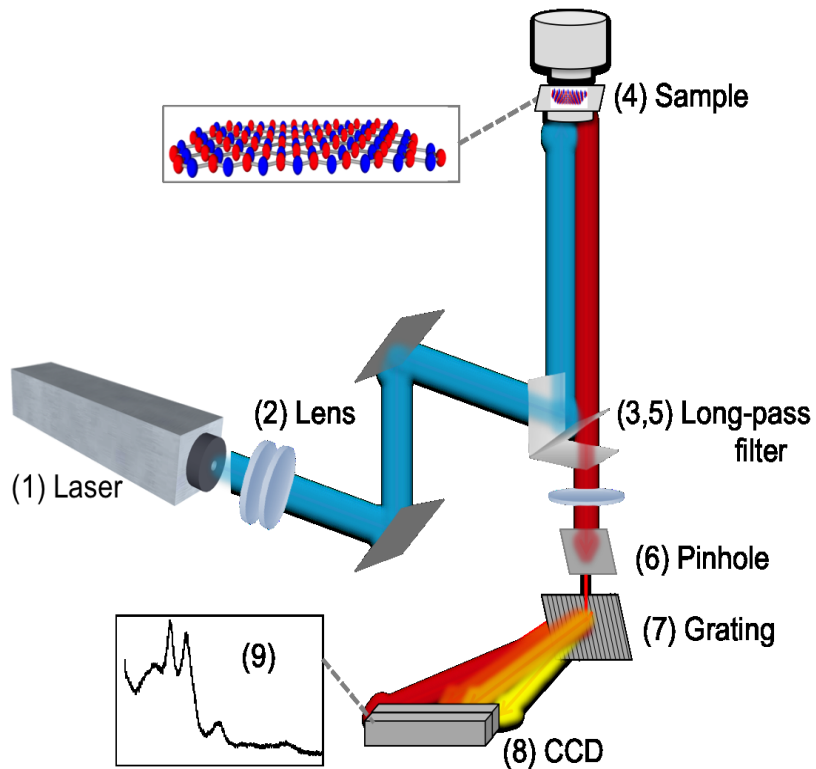
Figure 3.3: Illustration of a typical Raman microscopy setup. (1) Monochromatic excitation source (2) lens (3) the back of the long-pass filter is initially utilized as a mirror directing laser light towards the sample (4) sample material (5) long-pass filter removes laser line and weaker anti-stokes return (6) pin-hole serves to disperse scattered light (7) grating spreads out returned light onto CCD (8) Charge-coupled device (CCD) is utilized to electronically detect, record, and analysis returned spectra (9) the Raman spectra is displayed for further curve fitting and computer-based analysis.

The range of power output from the lasers varied from 1mW to above 20mW as measured at the sample surface allowing for the control of penetration of the laser light into the sample by scaling the source power output. For the purposes of this study a power output of ~1mW as measured at the sample surface was found to return optimal spectra. Increasing power allows for a shortened dwell time but also increases photonic interaction with the substrate, negating all attempts to try and minimize these peaks. By probing the sample at multiple wavelengths is possible to identify an appropriate wavelength that will avoid possible fluoresce across the substrate bandgap. For this study wavelengths of 488 nm, 514.5 nm, and 532 nm returned identifiable h-BN peaks with 488 nm being the optimal choice.

3.5.2 Grating & Slit Selection

Both a 2400 lines/mm and 3000 lines/mm gratings were utilized in this study interchanged between a 20 micron or 65 micron slit size to determine which setup allowed for the optimum amount of light. While combinations of both gratings and slit sizes yielded recognizable h-BN returns it was found that the most consistent and reliable set-up was the 3000 lines/mm grating with a 20 micron slit size. Choice of grating size affects both spectral range and fidelity given that each grating disperses the same. For instance, the 2400 lines/mm grating allows for a spectral measurement ranging from 0 to 1100 cm^{-1} while the 3000 lines/mm returns a spectral range of 0 to 950 cm^{-1}.
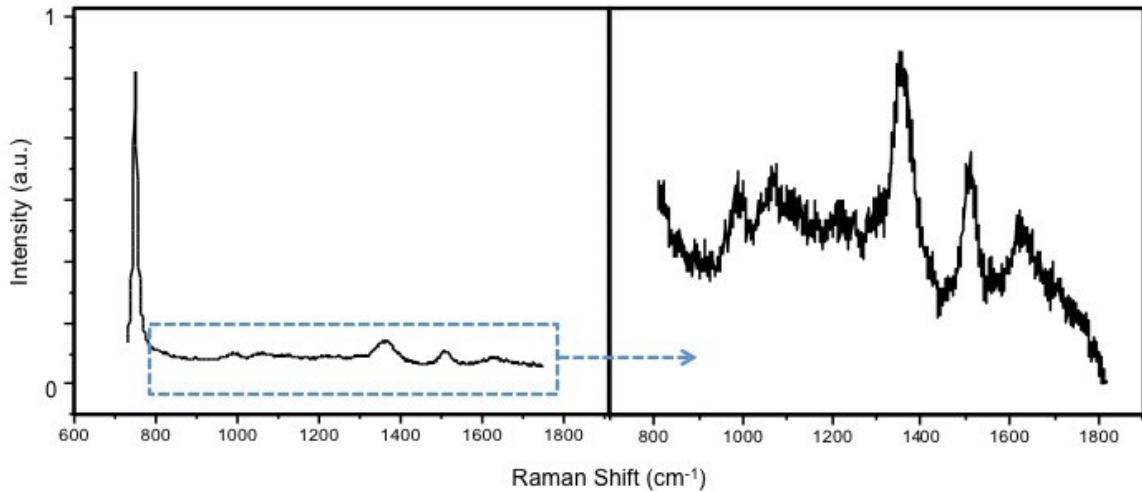
Figure 3.4: Side-by-side comparison of *h*-BN on sapphire spectra demonstrating the effects of preferentially centering gratings. (LEFT) Note that when the 3000 line/mm grating is centered at 1264 cm^{-1} the characteristic Al_2O_3 peak at 750 cm^{-1} drowns out the relatively weak 1367 cm^{-1} *h*-BN peak. Longer dwell times necessary for *h*-BN returns can often overload the CCD. (RIGHT) when the same 3000 line/mm grating is centered at 1336 cm^{-1} the Al_2O_3 peak is removed from the field-of-view allowing for a more prominent *h*-BN return.

Furthermore, not only does the 3000 lines/mm grating allow for a more focused and truncated spectral field-of-view, it also spreads that smaller area of spectral light out across the same amount of CCD pixels as opposed to lower numbered grating. This increases the ability of the CCD to detect weaker Raman peaks that otherwise would have been under-sampled with another grating setup.

3.5.3 Filtering

With the main Raman active peak of 1367 cm^{-1} the need for a near laser line filter was not particularly important, however, as discussed in the theory of Raman spectroscopy, the ability to filter out non-desired wavelengths generated by the excitation source greatly improves spectral resolution. A majority of filtering conducted in this

31

thesis was achieved through careful consideration of where to center the grating to avoid large substrate peaks that would "drown out" the inherently weak Raman returns from the *h*-BN film. Figure 3.4 demonstrates the importance of properly centering the grating to act as a "filter" against not only the laser line but also undesired and oversampled substrate peaks.

3.5.4 Objective Selection & Sampling Time

The highest objective available for Raman measurements utilizing the AFRL/RY Reinishaw inVia systems was 100 X allowing for a laser spot size of approximately 1 micron in diameter. Due to the layer thicknesses of ~1-10 nm the 100 X objective was the most widely utilized optical setup with the 50X being used sparingly. Any objective lower than 50 X (i.e. 20 X, 10 X, 5 X) resulted in purely substrate spectral returns without any discernible *h*-BN peaks. With <50 X objectives the laser spot size increases to a point where the substrate is oversampled to the point of drowning out any potential signal from a thin film.

Another key consideration when selecting an objective is the resulting laser spot size and depth of focus (DOF). DOF is the range over which a image is adequately within focus.

$$Spot\ size = \frac{1.22\lambda}{NA} \tag{7}$$

$$DOF = \frac{\lambda}{NA^2} \tag{8}$$

where the numerical aperture is denoted by NA and λ is the wavelength. It then follows that the highest objective available (100X in the case of this thesis) should be paired with

a sufficiently small wavelength to achieve a sufficiently small spot size and DOF to observe an atomically thin film on the order of nanometers.

To counteract the effect of undesirable laser penetration into the substrate it is possible to utilize a long dwell time of multiple signature accumulations to return an identifiable *h*-BN peak. For example, a one hour dwell time scan of a *h*-BN thin film would return a broad and weak *h*-BN peak (if any is observed) that is almost completely obscured by substrate effects. Instead of a single one hour dwell scan of the sample it is possible to utilize 60 one minute accumulations to help "draw out" the weaker *h*-BN peak while keeping any potential substrate effects minimized.

3.5.5 Calibration Techniques

Given the slight system fluctuations from day to day operations it is necessary to ensure proper calibration of the Raman system prior to any experimentation. The laser system was always turned on and allowed to achieve a stabilized power output prior to running a calibration sample. Silicon and diamond were used as reference materials for system calibration, due to their well-established Raman peaks at 520 cm^{-1} and 1336 cm^{-1}, respectively.

Laser power was measured ten times using an Edmonds Optics handheld laser power meter, with the highest and lowest measurement removed and the average of the remaining eight measurements would be recorded as the laser power for that day. The reference sample would then be placed on the microscope stage and brought into focus using the optical microscope at the objective to be used for that day's round of experiments (50X, 100X etc). Fifty accumulations with an integration time of one

second would then be taken at 100% laser power. These peaks are were then fit utilizing

built-in Reinishaw in-Via Wire 4.0 software to look for any fluctuations in the peak

position. The peak position and standard deviation were then recorded for later

reference.

3.6 Summary

This chapter presented references and explanations detailing the experimental and

procedural setup of investigating atomically thin h-BN films via Raman spectroscopy.

Investigation obstacles unique to 2D h-BN were discussed with the utilization of depth

profiling to preferentially sample surface films by focusing the laser beam slightly above

or below the substrate surface. The necessity to select a sufficiently high objective

magnification (i.e. 100 X) was found to be critical to reducing the laser spot size to ~1μm

in diameter allowing for sufficient excitation of the h-BN Raman active modes of the thin

film. Furthermore, the use of the 488 nm excitation source was found to return the most

consistent h-BN results given that the corresponding 2.54 eV excitation source was

approximately half of h-BN's 5.5 eV bandgap [5]. Consideration of proactively centering

the dispersion grating to avoid including large substrate peaks was also discussed (i.e.

centering a 3000 lines/mm grating at 1650 to avoid including the large broad silicon peak

at ~980 cm^{-1}).

IV. Results and Analysis

In this chapter, the results and analysis of the study are presented. An in-depth comparison of AFM measurements with collected Raman spectra is considered with respect to peak position, peak intensity, and full-width-half-maximum (FWHM). While twelve separately prepared samples of h-BN films were investigated on various substrates to include: Al_2O_3, copper foil, SiO_2, and SiO_2-backed copper foil, only results from one sample are presented below. The sample considered below was atomically thin h-BN on 300 nm thick SiO_2 on silicon (Si) substrate transferred via thermal release tape.

4.1 Selection and Designation of h-BN Sampled Areas

A high-powered optical microscope was used to conduct a preliminary investigation of the h-BN sample to identify areas where folding, wrinkling, or lift-off of the h-BN film had occurred. Although h-BN is transparent and undistinguishable by the naked eye it is possible to reveal surface features by altering the camera color filters and contrast ratios to represent topography. Figure 4.1 was obtained by maximizing the inVia Reinishaw's optical camera contrast ratio, eliminating green image color and over saturating the image's red hues. Utilizing these camera techniques it was possible to identify film folds and focus the Raman laser onto those specific areas as detailed in Figure 4.1.
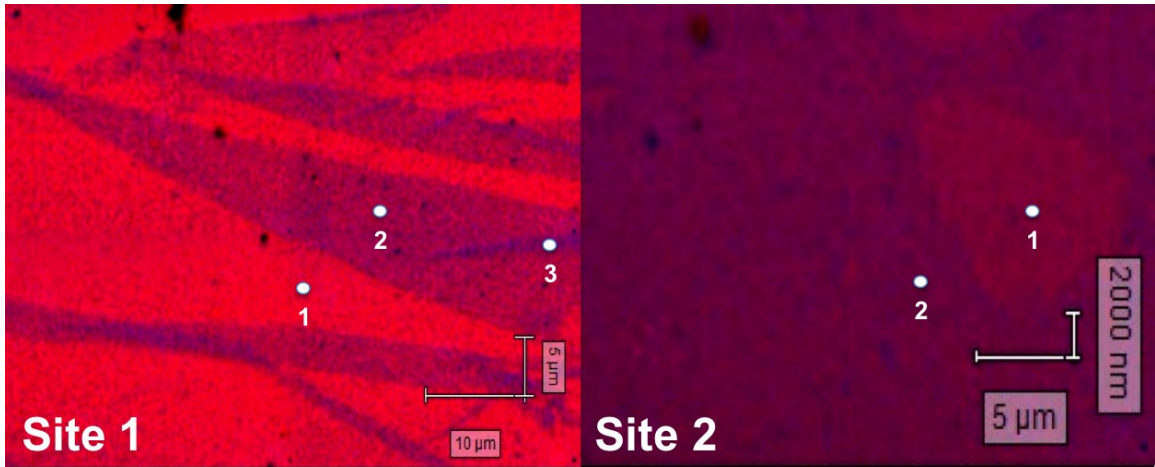
Figure 4.1: Optical microscope images of atomically thin h-BN film on SiO_2 at 100X magnification. (LEFT) Site 1 with three points of investigation called out to denote that the laser was focused on subsequently thicker areas of h-BN film. (RIGHT) Site 2 with its two points of interrogation denoted. Note that both images were adjusted for contrast with green filtering activated to allow for adequate recognition of the h-BN film.

The optical microscope was also used for a visual examination of the surface to note areas that had a noticeable presence of surface contaminates, such as carbon deposits due to the transfer process. These surface features allowed for a systematic investigation of the h-BN film at known incremental step increases of the film's thickness. Figure 4.1 illustrates the naming convention used in the subsequent Raman and AFM analysis to compare the two separate areas of the sample.

4.2 AFM Thickness Measurements

Figure 4.2 depicts two AFM images used to measure the topography of h-BN. Also noted in the figure are surface features that result from the transfer of the h-BN film from the copper growth catalyst to the SiO_2/Si substrate. These surface features are a result of tearing, folding, and wrinkling of the h-BN film. The varying film thicknesses

36

that arise due to the imperfections of the transfer process provided an ideal sample for the

Raman experimentation. Distinctive surface features were often used as reference points

to consistently find locations on the film for repeated experiments. The optical contrast

images were used to select locations with different thicknesses (later verified through

AFM) to be studied via Raman spectroscopy. They were exploited to take advantage of

the varying film thicknesses to allow for the investigation of any effects of Raman

spectral returns versus film thickness.
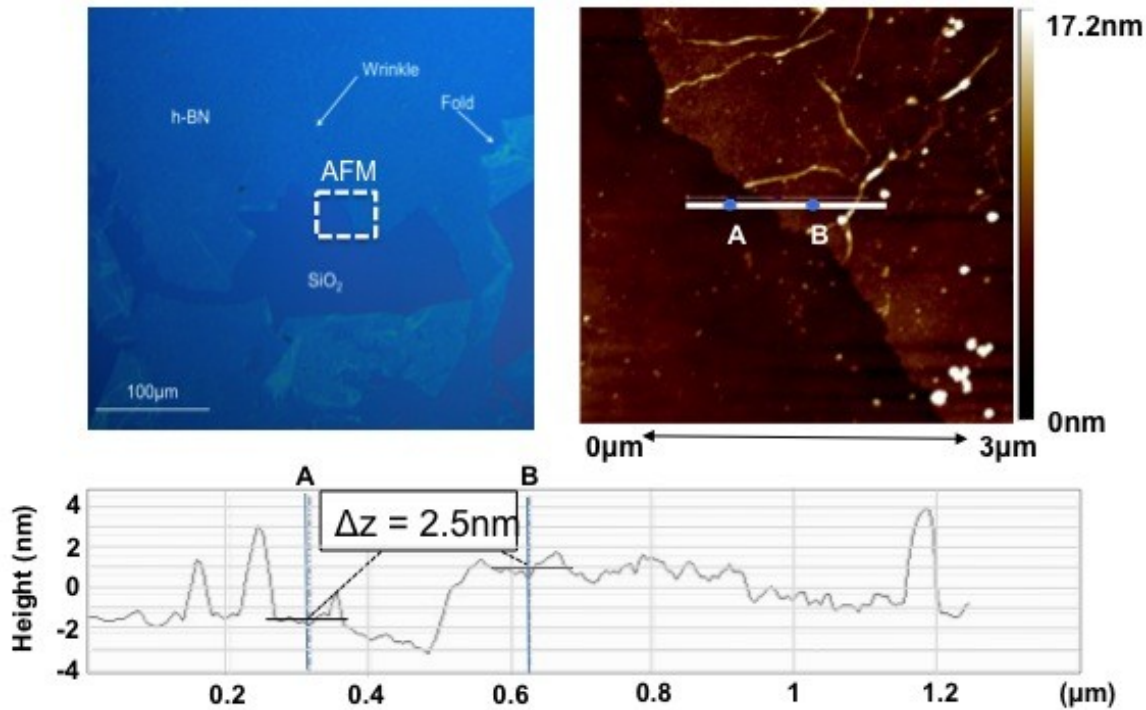
Figure 4.2: (UPPER LEFT) 100 X magnified image of h-BN film on SiO_2 denoting various surface features created during the film transfer to the substrate. (UPPER RIGHT) Blown-up AFM image of the h-BN film edge. (LOWER CENTER) AFM results signifying a 2.5 nm step between the substrate and the film corresponding to an approximate thickness of 7 atomic layers [34].
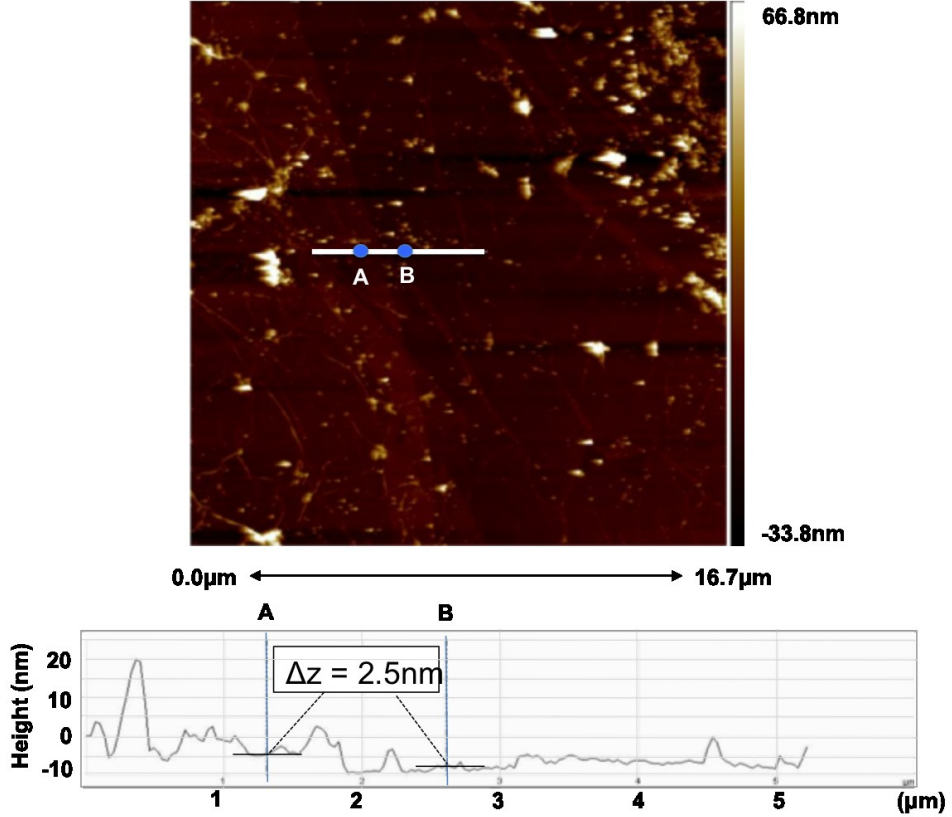
Figure 4.3: An AFM measurement of Site 1 of the *h*-BN film. Note that point A corresponds to a fold of the 2.5 nm *h*-BN film making point A approximately 5 nm thick (14 atomic layers). Point B corresponds to a single layer of *h*-BN film previously measured to be 2.5 nm thick (7 atomic layers).

The AFM measurements of Site 1, shown in Figure 4.3, show a step increase of 2.5 nm from the substrate onto the *h*-BN film. According to Chopra *et. al.* this corresponds to 7 atomic layers of AA' stacked *h*-BN [34]. It should be noted that water contamination can influence the AFM measurement such that the actual boron nitride layer is less than 7 atomic layers [27]. However, given the consistent 2.5 nm step on all three areas investigated via AFM it is reasonable to assume water contamination is not present.

The AFM images also indicate the presence of possible surface dust particles on the surface in both Figures 4.3 and 4.4. In the images these are identified as sharp concentrated anomalies. These surface particles are detectable in the optical images as white specks that lay along the denoted path (white line) traced by the AFM tip and were approximately 30nm in height. It is unlikely that these large surface features are a result of contamination due to their distinct and sharp increase and decrease in height. An inclusion contamination would push the h-BN upward causing a more gradual increase and decrease of the measured height.
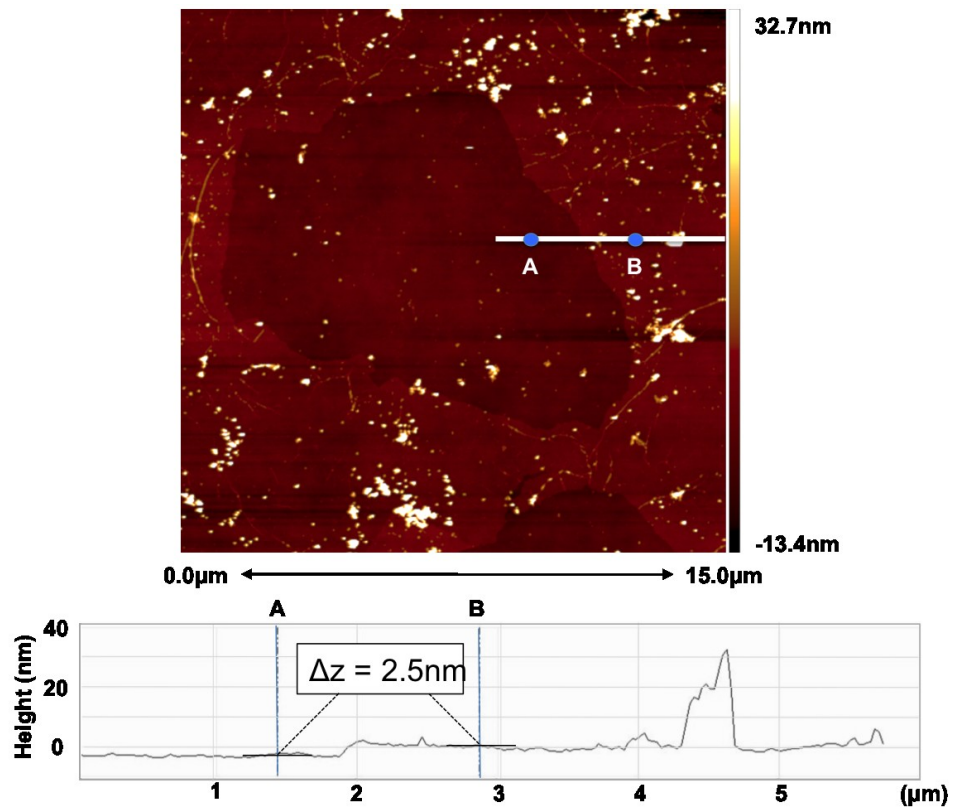

Figure 4.4: An AFM measurement Site 2 h-BN film. Note that point A corresponds to thickness of 0 nm because it lays in a hole in the h-BN film. Point B shows a step-up from Point A of 2.5 nm (7 atomic layers) corresponding to a single layer of h-BN film.

4.3 Raman Spectra of Atomically Thin *h*-BN and SiO$_2$

The first Raman spectra presented is of the bare SiO$_2$ substrate that the *h*-BN films were deposited onto. A careful consideration of the SiO$_2$ provides a useful point of contrast to the *h*-BN Raman spectra presented in Section 4.3.2 to help distinguish substrate effects from the *h*-BN signature. Section 4.3.2 provides the Raman spectra of the two areas of *h*-BN film investigated with the first area consisting of a hole and a single film step of 7 atomic layers and the second area consisting of 3 film steps at 7, 14, and 21 atomics layers.

4.3.1 Raman Analysis of SiO$_2$ Substrate

Raman spectroscopy was conducted on two separate sites of the same *h*-BN film sample. A 488 nm laser with a 3000 lines/mm grating was used to probe both the film and the substrate. The results for the substrate and film are presented separately. A wafer of 300 nm thick SiO$_2$ on silicon was chosen as a substrate to investigate *h*-BN given silicon oxide's well-known Raman spectra and it's atomically smooth surface. As seen in Figure 4.5, a drawback to using SiO$_2$ as a substrate is the presence of a combination peak at 1369.7 cm^{-1} exactly where the characteristic *h*-BN 1367 cm^{-1} peak is to be investigated.
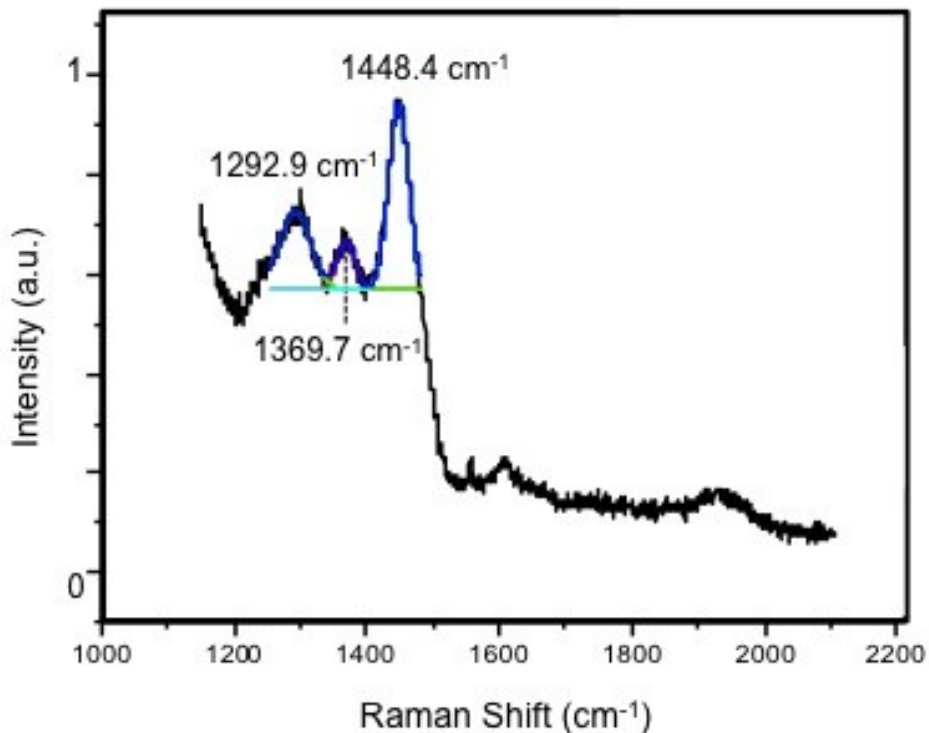
Figure 4.5: Raman spectra of a 300 nm SiO_2 substrate used for *h*-BN investigation. Note that the location of a combination silicon and SiO_2 peak is present at 1369.7 cm^{-1}, in the same location as the characteristic E_{2g} peak for *h*-BN. [Spectra was obtained after 30 accumulations of 60 second exposures using a 488 nm Argon ion laser with 1.12mW measured power at sample with 20μm slits, 100X objective, 3000 lines/mm grating centered at 1650 cm^{-1}]

As discussed in Chapter 2, another drawback to using SiO_2 on silicon as a *h*-BN substrate is the necessity to center the grating at 1650 cm^{-1} to avoid overloading the CCD with the highly Raman active silicon peak at approximately 920 cm^{-1} given the long dwell time needed to return an atomically thin *h*-BN Raman signature peak. Long dwell times can potentially lead to sample heating which could in turn damage the *h*-BN. Given the strong interatomic bonding of *h*-BN and its use in industrial high-heat applications sample heating becomes secondary concern behind achieving adequate Raman returns.

41

4.3.2 Spectral Returns of Sites #1 and #2

All spectral returns were taken at a depth to maximize 1367 cm^{-1} *h*-BN peak intensity as determined by a depth profiling of the sample area. By normalizing all spectral returns to a maximized *h*-BN 1367 cm^{-1} peak an objective comparison of separate film thicknesses was achieved. Figures 4.6 and 4.7 (next page) show the observed Raman spectra of Site 1 and 2, respectively. Figure 4.6 shows the spectral returns of 3 separate points of Site 1 of increasing thickness with an independently AFM ascertained change of film thickness of 2.5 nm from Pt 1 (thinnest, 2.5 nm, 7 atomic layers) to Pt 3 (thickest, 7.5 nm, 21 atomic layers) with Pt 2 being between both Pt 1 and 3 at a thickness of 5 nm or 14 atoms. Similarly, Figure 4.7 details the spectral return of 2 separate points of Site 2 with Pt 1 corresponding to at hole in the *h*-BN film (revealing the SiO$_2$ substrate) and Pt 2 corresponding single layer thick measured at 2.5 nm or 7 atoms thick.
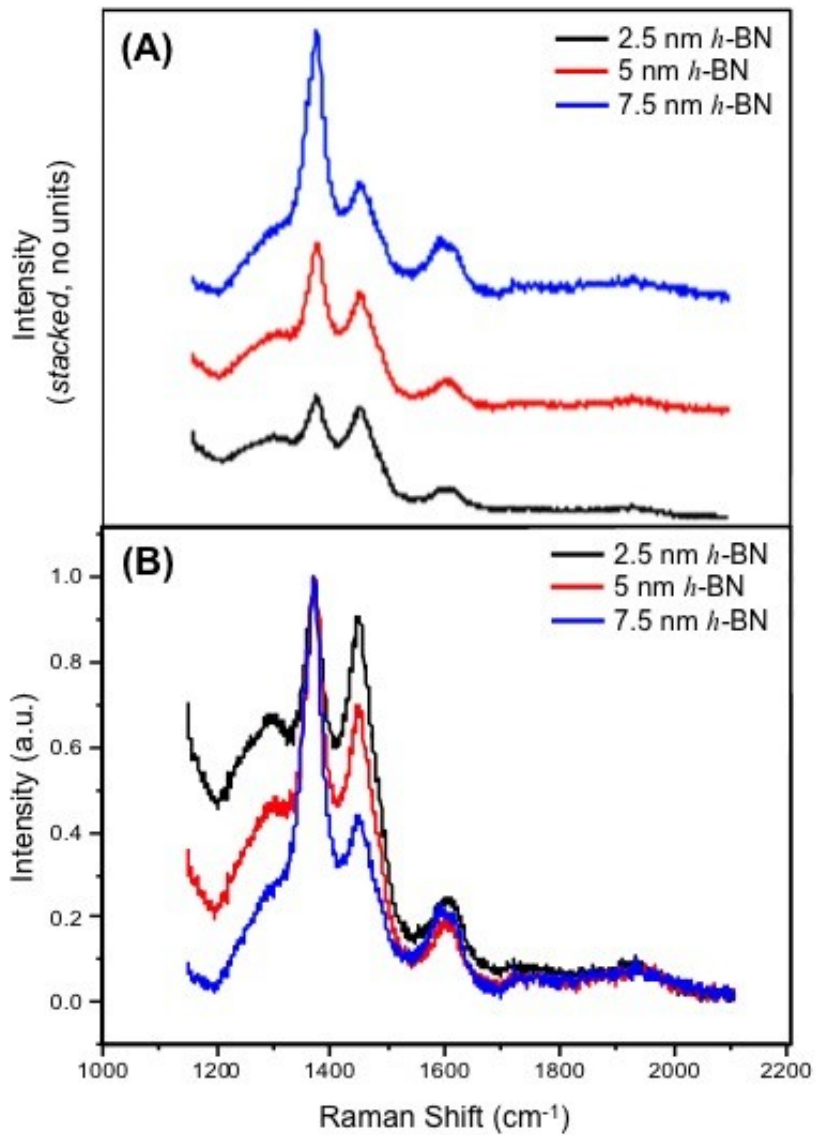
Figure 4.6: Raman spectrums of Site 1 of atomically thin *h*-BN film on SiO$_2$. (A) Pt 1, Black: thinnest area of film measured, 2.5 nm (7 atoms); Pt 2, Red: 2 layers of *h*-BN film, 5 nm (14 atoms); Pt 3, Blue: 3 layers of *h*-BN film, 7.5 nm (21 atoms). (B) Depiction of chart A normalized to the *h*-BN peak. [Spectra was obtained after 30 accumulations of 60 second exposures using a 488 nm Argon ion laser with 1.12mW measured power at sample with 20μm slits, 100X objective, 3000 lines/mm grating centered at 1650 cm^{-1}]
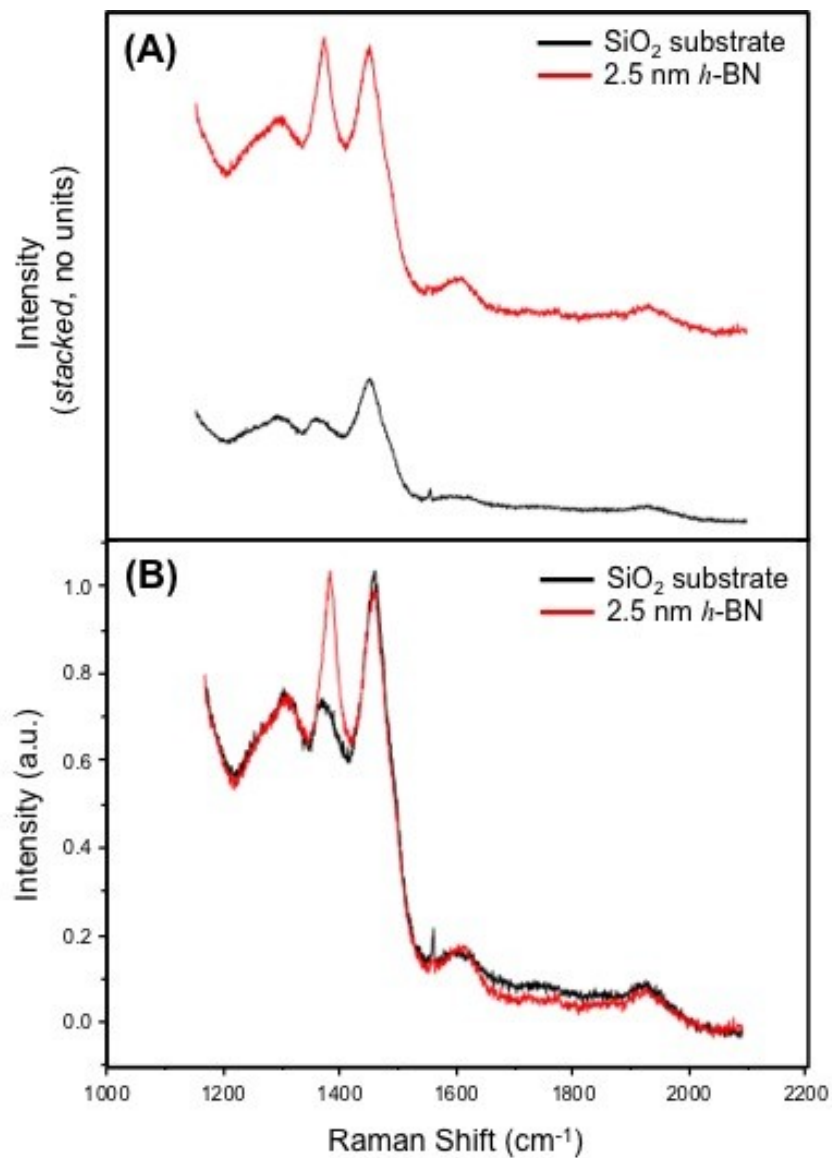
Figure 4.7: Raman spectrums of Site 2 of atomically thin *h*-BN film on SiO$_2$. (A) Pt 1, Black: hole in the *h*-BN film revealing the SiO$_2$ substrate; Pt 2, Red: single layer of *h*-BN film 2.5 nm thick (7 atoms). (B) Depiction of chart A normalized to the *h*-BN peak. [Spectra was obtained after 30 accumulations of 60 second exposures using a 488 nm Argon ion laser with 1.12mW measured power at sample with 20μm slits, 100X objective, 3000 lines/mm grating centered at 1650 cm^{-1}]

As one would expect there is a noted increase to the 1367 cm^{-1} h-BN peak as the film thickness increases allowing for a stronger Raman return from the deposited film. Next to this 1367 cm^{-1} h-BN peak increase the 1448 cm^{-1} SiO_2 looks as though it is diminishing. However as can be seen in Figure 4.6 (A) the SiO_2 remains constant throughout each of the separate scans. It is this persistence of a SiO_2 substrate peak that that can be used as a point of reference from which to investigate any changes to the intensity of the 1367 cm^{-1} h-BN peak. This idea is explored further in the next section.

4.4 Effect of Film Thickness on Raman Spectra

Figure 4.8 (next page) provides and overlay of the Raman spectra of both Site 1 and 2 at all thicknesses measured. With all the spectra stacked together it is evident that both the green spectra (Site 2, Pt 2) and the black spectra (Site 1, Pt 1) are strongly correlated. When normalized to the SiO_2 peak Site 2 Pt 2 yielded a 1.02 peak ratio which closely compares to the 1.06 peak ratio found for Site 1 Pt 1. A complete analysis of the various peak ratios can be seen in Table 4.1 in the subsequent section.
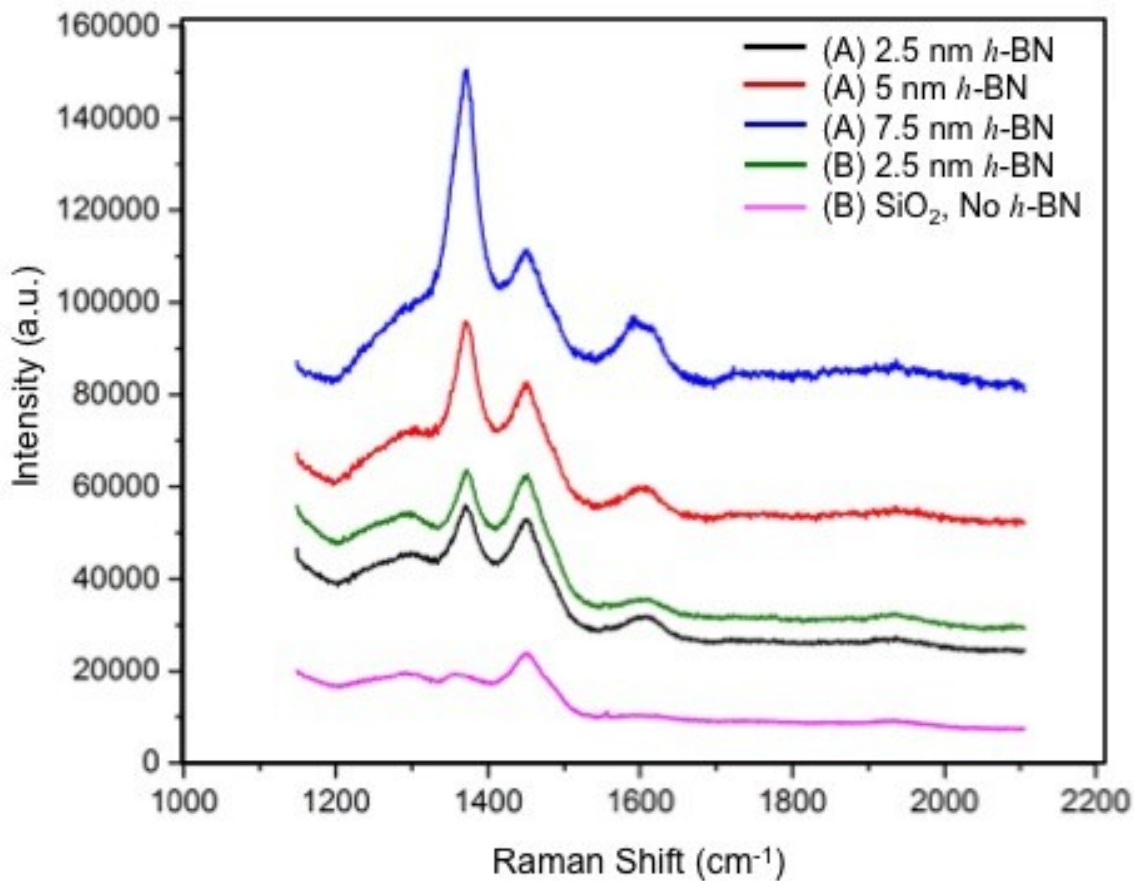
Figure 4.8: Unaltered spectral return of both Site 1 (A) and Site 2 (B). As to be expected the relative intensity of the Raman spectra increases with increases of film thickness. Note the high correlation of two single layers of *h*-BN examined between Site 1 & 2 and the dependence of the 1367 cm^{-1} *h*-BN peak on film thickness.

Figure 4.9 removes the redundant single layer spectra line from Site 2 to demonstrate the lack of any blue-shifting as a function of thickness to the characteristic E_{2g} *h*-BN peak, seen in Figure 4.9 at 1369 cm^{-1}. A marked increase to both the 1367 cm^{-1} *h*-BN peak intensity and a tightening of the full-width half-maximum with the thickening of the *h*-BN film can be seen in the magnified area of Figure 4.9 (however, no correlation in the FWHM can be mathematically shown). The pink spectra denoting the SiO_2

substrate shows a broad red-shifted peak that had previously been seen at 1369.5 cm^{-1} as shown in Figure 4.5. A comparison of this broad SiO$_2$ peak (observed in Figure 4.9 at approximately 1358 cm^{-1}) with the stronger 1448 cm^{-1} neighboring peak serves to confirm the ability of Raman spectroscopy to distinguish between the substrate and presence of a *h*-BN surface film.
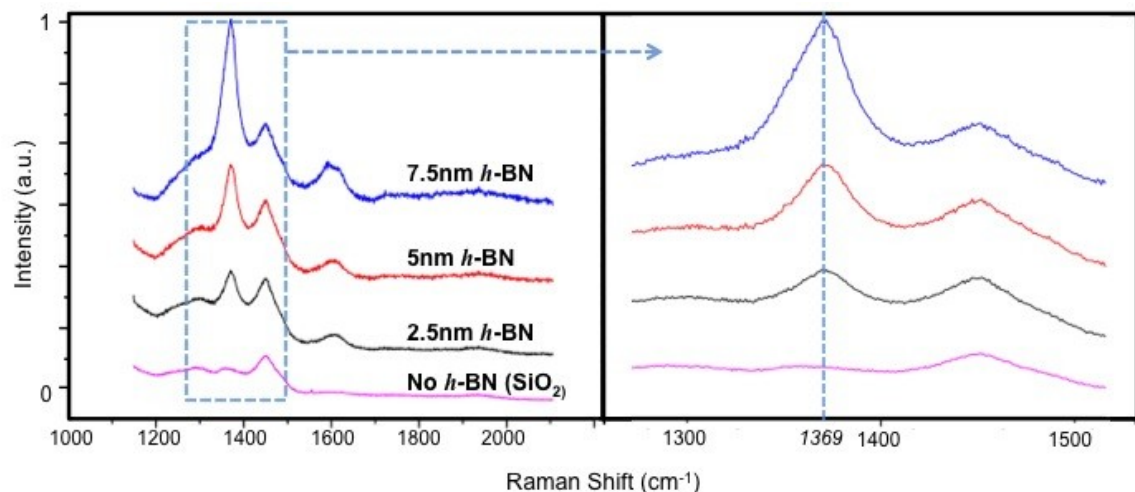
Figure 4.9: Figure 4.8 with the redundant single layer Site 2 Raman spectra removed. Note on the right-hand magnified region that all 3 of the *h*-BN spectra show no shifting of the 1367 cm^{-1} E$_{2g}$ peak with a change in thickness (seen here at 1369 cm^{-1} due to possible material strain or system calibration shifting).

To further investigate the relationship between the E$_{2g}$ *h*-BN peak and 1448 cm^{-1} SiO$_2$ peak it was helpful to normalize all four spectra to common reference point. To this end the SiO$_2$ peak was held stationary to allow for a clear understanding of how the E$_{2g}$ peak changed with film thickness. As can be seen in Figure 4.10 when the 1448 cm^{-1} SiO$_2$ peak is normalized to 1 the corresponding intensity of the SiO$_2$ substrate at 1369 cm^{-1} is 0.81. When a single layer of 2.5 nm thick *h*-BN film is introduced the 1369 cm^{-1}

peak is 1.06 as compared to the SiO_2 peak. When a double and triple layer of h-BN is analyzed the ratio increases to 1.16 and 1.35, respectively. Given the previously mentioned correlation of 1.02 and 1.06 between the two single h-BN layers investigated there is high likelihood that film thickness can be determined exclusively through a careful consideration of the characteristic E_{2g} h-BN peak with a reference substrate peak (such as the 1448 cm^{-1} peak SiO_2 peak).
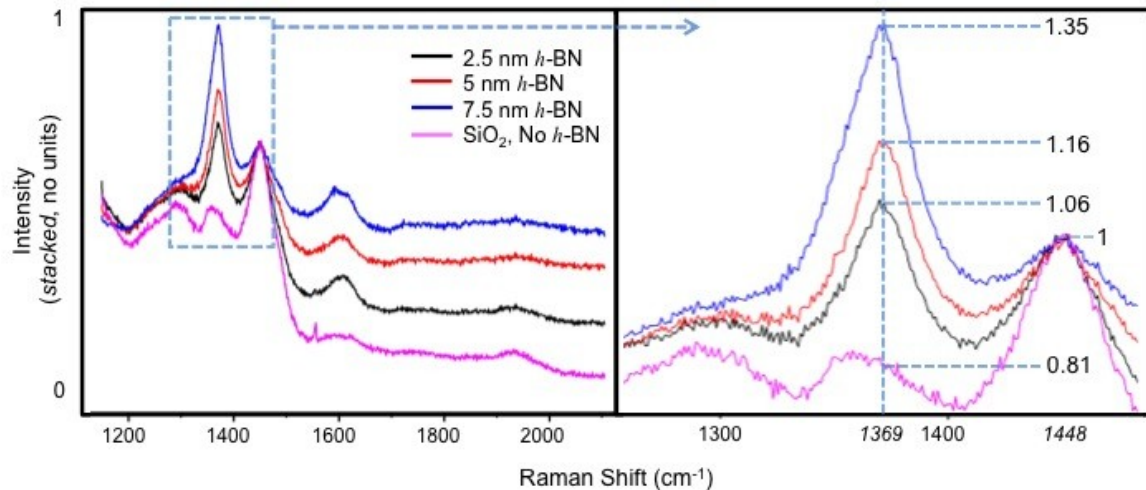
Figure 4.10: The same spectra shown in Figure 4.9 normalized to the 1448 cm^{-1} SiO_2 peak to show for the h-BN peak intensity changes with film thickness relative to reference point (SiO_2). Normalized ratios for each of the 4 spectra at 1369 cm^{-1} (the same 1369 cm^{-1} point was taken on the broad amorphous SiO_2 substrate peak to establish a reference datum).

The peak intensity ratios are plotted against atomic thickness in Figure 4.11 with a linear regression fitted to the data as denoted below,

$$y = 0.0265x + 0.8084 \qquad (9)$$

$$R^2 = 0.9986.$$

48

The y-intercept describes the native ratio of the SiO_2 1448 cm^{-1} used as a normalization point to the intensity of the SiO_2 substrate observed at 1369 cm^{-1} to provide a datum reference for the introduction of subsequent *h*-BN layers to the substrate. The strong 0.9986 R^2 (chi-squared) suggests that the relationship between peak intensity and film thickness is linear, however, it can be observed that the one layer data point at 1.06 lays above the best fit line revealing that further research and data collection will be necessary to refine any potential relationship.
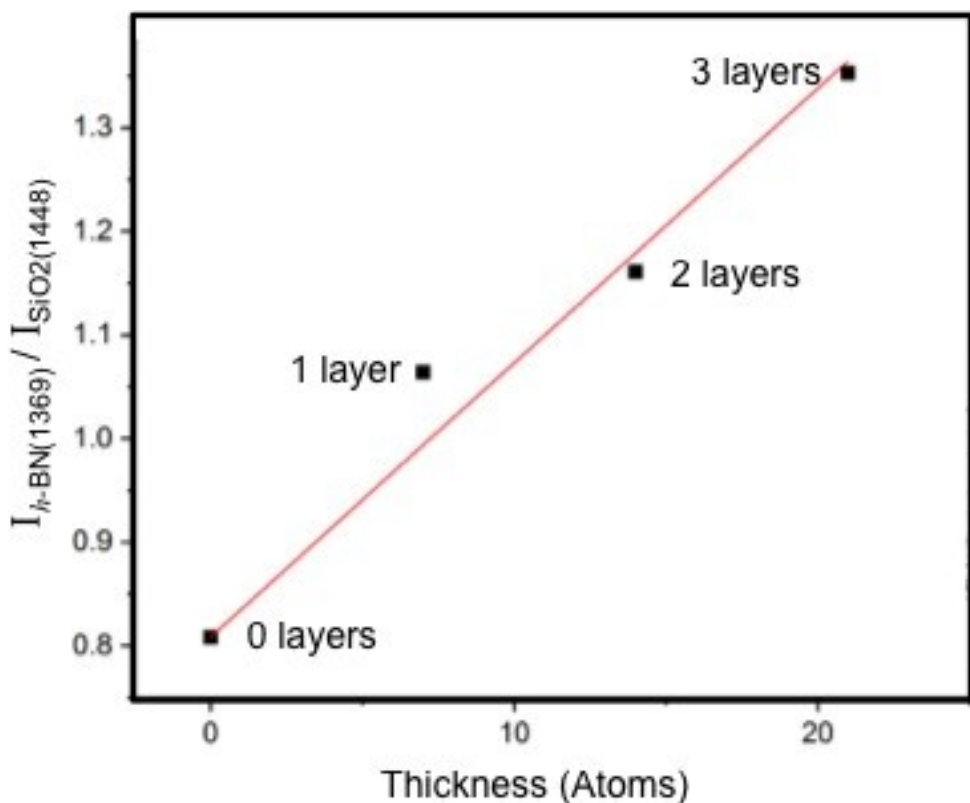
Figure 4.11: The relative peak intensities of the 1369 *h*-BN peak to their corresponding 1448 cm^{-1} SiO_2 reference peak as a function of atomic thickness. Linear fit line equation of y=0.0265x+0.8084 with an R^2 value of 0.9986.

49

Presented in Chapter 2 the research conducted by Gorbachev et. al. of the Manchester group suggested that an upshift (or blueshifting) of the characteristic 1367 cm^{-1} E$_{2g}$ h-BN peak of approximately 4 cm^{-1} could be observed with atomically thin films [27]. However, this upshift was not observed during the course of this thesis or in a similar examination by Ismach *et. al*. of the University of Texas, Austin [7]. Across both samples the h-BN peak ranged from 1368.5 cm^{-1} (7 atomic layers) to 1369.1 cm^{-1} (14 atomic layers). The location of the E$_{2g}$ peak at 1369 cm^{-1} instead of the classically accepted 1367 cm^{-1} for bulk h-BN is unlikely caused by the laser line being offset from the grating as discussed in Chapter 3. It is possible that there was some residual strain in the h-BN film as well which could have caused a slight 1-2 cm^{-1} upshift to the h-BN peak. The film could easily have been strained due to the folding and wrinkling surface features used to identify areas of various thicknesses.
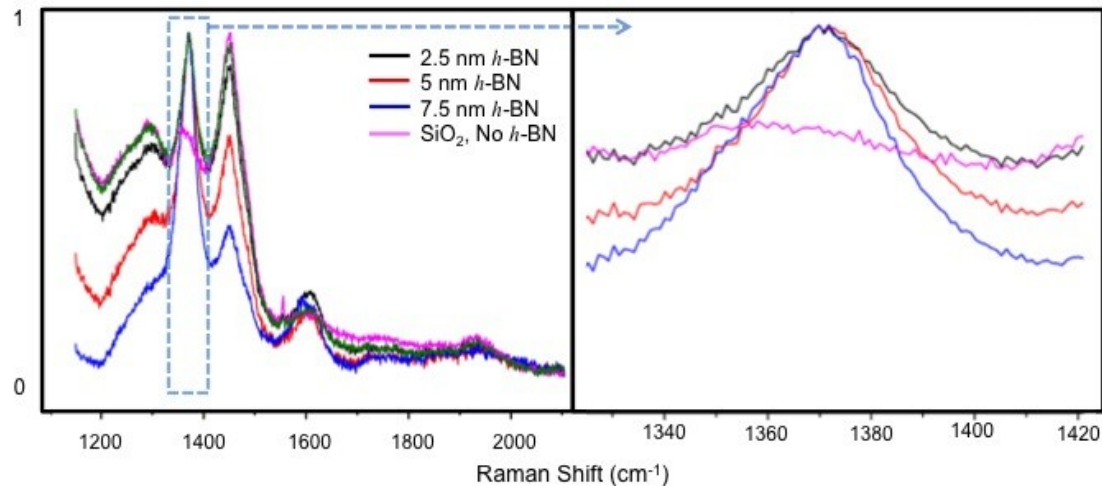
Figure 4.12: h-BN spectra normalized to 1 and magnified about the 1367 cm^{-1} peak to emphasize the lack of peak shifting in the E$_{2g}$ peak as well as the peak tightening with film thickness.

4.5 Peak Fitting

A traditional Gaussian fitting algorithm within the Origin Pro 8 software was used to analyze both the boron nitride and SiO_2 peaks had R^2 values in excess of 0.97. The broad subdued peak at approximately 1600 cm^{-1}, attributed to carbon deposits from the use of thermal release tape in the transfer process [35], were not analyzed.

Possible sources of error to the *h*-BN 1367 cm^{-1} being blue-shifted 1-2 wavenumbers include both the previously observed 1369.7 cm^{-1} SiO_2 peak present in the substrate as well as the relatively weak signal of the principal peaks. As a best practice, any Raman peak of intensity less than 20,000 counts would be considered subject to slight peak shifting, similar to the method used to calibrate the system to diamond as discussed in Chapter 3.
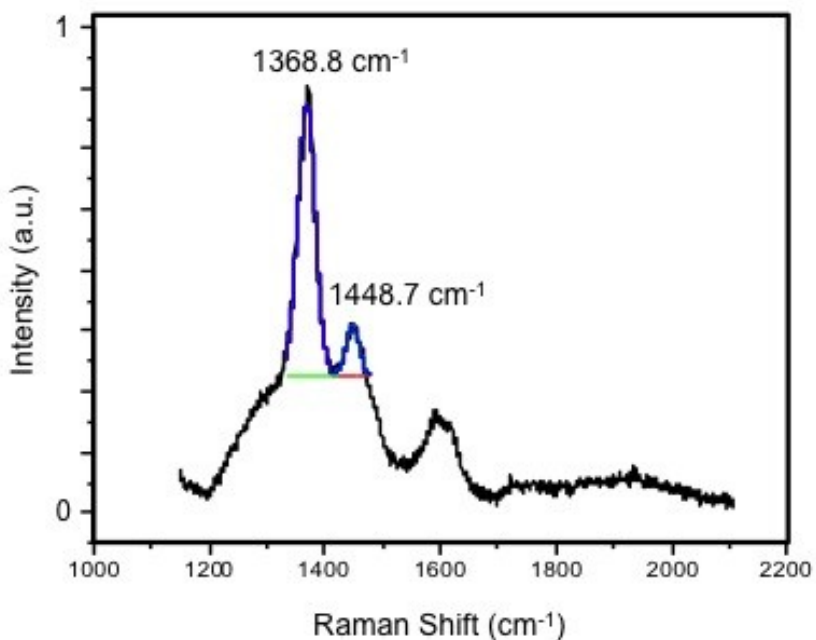
Figure 4.13: Example of peak fitting routine of Site 1 point 3 (7.5 nm thick) utilized for spectral analysis of the examined thin films.

4.6 Table of Peak Data

The aggregate data from both Sites 1 and 2 has been compiled into Table 1 denoting observed peak positions of both the h-BN E_{2g} and SiO_2 1448 cm^{-1} peaks, fitted full width half max (FWHM), number of counts detected per peak, R-squared linear regression scores and the intensity ratio of the h-BN E_{2g} to the SiO_2 1448 cm^{-1} peaks. No distinguishable correlation between the FWHM and film thickness was noted with values ranging from 30.8 to 34.6.

Table 1: Table of compiled peak data for atomically thin h-BN film on SiO_2 substrate for Sites 1 & 2 at each reference point.

		h-BN					SiO_2				
		Thickness (atoms)	(nm)	Position (cm^{-1})	FWHM	Counts	Position (cm^{-1})	FWHM	Counts	Intensity ($^{h\text{-}BN}/_{SiO_2}$)	R^2
Site 1	Pt 1	7	2.5	1369.0	32.0	55,996	1448.1	28.9	52,901	1.06	0.972
	Pt 2	14	5	1369.1	30.8	95,937	1448.6	27.8	82,630	1.16	0.986
	Pt 3	21	7.5	1368.8	34.4	150,429	1448.7	23.7	111,334	1.35	0.991
Site 2	Pt 1	0	0	n/a (1363)	n/a	19,125	1447.9	34.6	23,658	0.81	0.971
	Pt 2	7	2.5	1368.5	34.6	63,124	1448.2	26.8	62,069	1.02	0.990

4.7 Summary

Chapter 4 presented the results and analysis of this thesis with regards to two separate areas of atomically thin h-BN deposited onto a 300 nm thick SiO_2 substrate. Initial AFM measurements of both regions showed a step increase of 2.5 nm from one layer of h-BN to another denoting a film thickness of approximately 7 atomic layers [34]. The first h-BN area investigated via Raman spectroscopy was probed at three distinct points of increasing thickness revealing a decreasing ratio of the SiO_2 substrate peak to

the E_{2g} h-BN peak of 1.06, 1.16, and 1.35, respectively. The second area with a hole in the h-BN film was investigated at two distinct points, one point in the middle of the hole revealing the SiO_2 substrate and the second point next to the hole on a single layer of boron nitride film. The single layer h-BN point had a peak ratio of 1.02, which agreed well with the previously measured single layer peak ratio of 1.06. Plotting the peak ratios yielded a linear relationship of $y = 0.0265x + 0.8084$. The full-width half maximum values of the characteristic h-BN peak ranged from 30.8 to 35.6 across both sites and showed no correlation with film thickness. Similarly, the characteristic 1367 cm^{-1} E_{2g} h-BN peak ranged from 1368.5 cm^{-1} to 1369.1 cm^{-1} with no evident shift due to increasing film thickness.

V. Conclusion

The principal objective of this thesis was to explore the ability of Raman spectroscopy to provide an in-depth non-destructive method of characterizing atomically thin h-BN films. This research was motivated in large part by the research presented by Gorbachev *et. al*. in "Hunting for Monolayer Boron Nitride: Optical and Raman Signatures" detailing the potential ability of Raman spectroscopy to determine the number of layers in mono-to-few layer thick h-BN films through an upshift of the characteristic E_{2g} h-BN peak [27]. Having investigated two separate regions of h-BN films ranging from 0 to 7.5 nm thick via Raman spectroscopy the characteristic E_{2g} h-BN peak showed a range of 1368.5 cm^{-1} to 1369.1 cm^{-1} with no evident upshift due to increasing film thickness. Furthermore, no correlation between the full-width half-maximum and increasing film thickness was found. The FWHM values ranged from 30.8 to 35.6 across both sites sampled. A linear relationship of $y = 0.0265x + 0.8084$ with a R^2 of 0.9986 (with x being in atoms) was observed between the 1367 cm^{-1} E_{2g} h-BN and 1448 cm^{-1} SiO_2 peak intensities. This suggests that the thickness of an atomically thin h-BN film may be determined through a careful investigation of the peak intensity when normalized to a substrate reference peak.

A secondary conclusion of this thesis was the best practice of repeatedly isolating a h-BN Raman signal, a problematic process. The system set-up consisted of: the highest fidelity grating available to the laboratory (3000 lines/mm) centered to minimize any strong substrate returns, a long-pass filter; 20 micron slits; and the 488 nm excitation source in excess of 1mW (measured at sample) was found to optimal. Excitation sources

below this failed to return a discernible E_{2g} h-BN peak and excitation sources above 514 nm caused strong luminescence in the returned spectra.

5.1 Future Research

Future research could include a systematic investigation of multiple h-BN film samples via AFM to create a catalog of ever increasing film thicknesses (ideally ranging from mono-layer to approximately 20 atomic layers) that could then be investigated via Raman spectroscopy to correlate integer atomic steps to layer thickness with a corresponding increase to the characteristic E_{2g} h-BN peak. Through an exhaustive population of Figure 4.10 a true best fit line and linear relationship may be established. This exercise should be carried out across multiple substrates to investigate if similar reference peaks analogous to the SiO_2 1448 cm^{-1} peak can be exploited for thickness measurements.

Furthermore, this thesis utilized long single dwell Raman scans at surface depths determined through depth profiling to return the strongest h-BN signatures. Given the micron-level resolution of the Raman system's step motor it may be advantageous to extend the dwell time of the depth profiles and use these returns in place of single long scan. This would allow for a higher level of certainty that the investigated h-BN signal has been maximized to optimal level of return. Other areas for research beyond the thickness measurement the h-BN film would be further exploration of how to produce h-BN films free of contaminates introduced during the transfer process. One method currently being investigated by AFRL/RY is the employment of "ashing" via an ionized oxygen to remove any carbon deposits on the surface.

Another potential area of investigation would be an in-depth analysis of the 52.5 cm^{-1} *h*-BN shear mode as a function of film thickness. Preliminary scans done during the course of this thesis did not return a discernible shear mode peak. However, a more deliberate round of Raman scans with a near laser line filter (such as the NExT filter) may provide more promising results. By filtering out the laser line and conducting a low-wavenumber Raman analysis of *h*-BN one should be able to gain an understanding of the shearing acoustic modes which will shed insight into the material's stacking order and defect concentration. It is not unreasonable to predict that the shear mode would be highly correlated to film thickness, even more so than the high energy mode.

References

1.   F. Schwierz, "Graphene transistors.," *Nat. Nanotechnol.*, vol. 5, no. 7, pp. 487–96, Jul. 2010.

2.   C. R. Dean, A. F. Young, I. Meric, C. Lee, L. Wang, S. Sorgenfrei, K. Watanabe, T. Taniguchi, P. Kim, K. L. Shepard, and J. Hone, "Boron nitride substrates for high-quality graphene electronics.," *Nat. Nanotechnol.*, vol. 5, no. 10, pp. 722–6, Oct. 2010.

3.   K. I. Bolotin, K. J. Sikes, J. Hone, H. L. Stormer, and P. Kim, "Temperature-Dependent Transport in Suspended Graphene," *Phys. Rev. Lett.*, vol. 101, no. 9, p. 096802, Aug. 2008.

4.   K. Watanabe, T. Taniguchi, and H. Kanda, "Direct-bandgap properties and evidence for ultraviolet lasing of hexagonal boron nitride single crystal.," *Nat. Mater.*, vol. 3, no. 6, pp. 404–9, Jun. 2004.

5.   A. K. Geim and K. S. Novoselov, "The rise of graphene," *Nat. Mater.*, vol. 6, no. March 2007, pp. 183–191, 2007.

6.   R. Quhe, J. Zheng, G. Luo, Q. Liu, R. Qin, J. Zhou, D. Yu, S. Nagase, W.-N. Mei, Z. Gao, and J. Lu, "Tunable and sizable band gap of single-layer graphene sandwiched between hexagonal boron nitride," *NPG Asia Mater.*, vol. 4, no. 2, Feb. 2012.

7.   A. Ismach, H. Chou, D. a Ferrer, Y. Wu, S. McDonnell, H. C. Floresca, A. Covacevich, C. Pope, R. Piner, M. J. Kim, R. M. Wallace, L. Colombo, and R. S. Ruoff, "Toward the controlled synthesis of hexagonal boron nitride films.," *ACS Nano*, vol. 6, no. 7, pp. 6378–85, Jul. 2012.

8.   H. Pedersen, C. Höglund, J. Birch, J. Jensen, and A. Henry, "Low Temperature CVD of Thin, Amorphous Boron-Carbon Films for Neutron Detectors," no. 18, pp. 221–224, 2012.

9.   H. Wang, T. Taychatanapat, A. Hsu, K. Watanabe, T. Taniguchi, P. Jarillo-Herrero, and T. Palacios, "BN/Graphene/BN Transistors for RF Applications," *IEEE Electron Device Lett.*, vol. 32, no. 9, pp. 1209–1211, Sep. 2011.

10.   K. Shinohara, Y. Yamashita, A. Endoh, K. Hikosaka, T. Matsui, T. Mimura, and S. Hiyamizu, "Ultrahigh-speed pseudomorphic InGaAs/InAlAs HEMTs with 400-GHz cutoff frequency," *IEEE Electron Device Lett.*, vol. 22, no. 11, pp. 507–509, Nov. 2001.

11.   A. P. Express, "InGaAs buffer / channel structure boosts effective," *Semicond. Compd. Adv. Silicon*, vol. 6, no. 10, 2012.

12. L. Britnell, R. V. Gorbachev, R. Jalil, B. D. Belle, F. Schedin, A. Mishchenko, T. Georgiou, M. I. Katsnelson, L. Eaves, S. V. Morozov, N. M. R. Peres, J. Leist, A. K. Geim, K. S. Novoselov, and L. Ponomarenko, "Field-effect tunneling transistor based on vertical graphene heterostructures.," *Science*, vol. 335, no. 6071, pp. 947–50, Feb. 2012.

13. D. Palmer, "THz Electronics Program Images Additional Information." [Online]. Available: http://www.darpa.mil/Our_Work/MTO/Programs/THz_Electronics.aspx. [Accessed: 07-Oct-2013].

14. R. Geick, C. Perry, and G. Rupprecht, "Normal modes in hexagonal boron nitride," *Phys. Rev.*, vol. 146, no. 2, 1966.

15. T. Kuzuba, K. Era, T. Ishii, and T. Sato, "A Low Frequency Raman-Active Vibration of Hexagonal Boron Nitride," *Solid State Commun.*, vol. 25, pp. 863–865, 1978.

16. C. Kittel, *Introduction to Solid State Physics*, vol. 21, no. 8. 1953, p. 650.

17. K. S. Novoselov, D. Jiang, F. Schedin, T. J. Booth, V. V Khotkevich, S. V Morozov, and A. K. Geim, "Two-dimensional atomic crystals," *PNAS*, vol. 102, no. 30, pp. 10451–10453, 2005.

18. K. S. Novoselov, A. K. Geim, S. V Morozov, D. Jiang, Y. Zhang, S. V Dubonos, I. V Grigorieva, and A. A. Firsov, "Electric field effect in atomically thin carbon films.," *Science*, vol. 306, no. 5696, pp. 666–9, Oct. 2004.

19. Y. M. Lin, K. a Jenkins, A. Valdes Garcia, J. P. Small, D. B. Farmer, and P. Avouris, "Operation of graphene transistors at gigahertz frequencies.," *Nano Lett.*, vol. 9, no. 1, pp. 422–426, Jan. 2009.

20. G. Turrell and J. Corset, *Raman Microscopy: Developments and Applications*, 1st ed. Elsevier Academic Press, 1996, p. 463.

21. A. Smekal, "Zur Quantentheorie der Dispersion," *Naturwissenschaften*, vol. 11, no. 43, pp. 873–875, Oct. 1923.

22. C. Raman, "Nobel Lecture: The molecular scattering of light." Stockholm, Sweden, 1930.

23. D. C. Harris and M. D. Bertolucci, *Symmetry and Spectroscopy: An Introduction to Vibrational and Electronic Spectroscopy*. Courier Dover Publications, 1978, p. 550.

24. E. Smith and G. Dent, *Modern Raman Spectroscopy: A Practical Approach*. Wiley, 2006, p. 224.

25.   A. B. Kaul, E. W. Wong, L. Epp, and B. D. Hunt, "Two-dimensional atomic layered materials and their applications," *Nano Lett.*, vol. 6, no. 5, pp. 942–7, May 2006.

26.   M. G. Beghi, C. E. Bottani, A. Miotello, and P. M. Ossi, "Vibrational spectroscopy of mixed hexagonal-cubic boron nitride thin films," *Thin Solid Films*, vol. 309, pp. 107–112, 1997.

27.   R. Gorbachev, I. Riaz, R. Nair, and R. Jalil, "Hunting for Monolayer Boron Nitride: Optical and Raman Signatures," *Small*, pp. 1–5, 2011.

28.   S. Reich, a. Ferrari, R. Arenal, a. Loiseau, I. Bello, and J. Robertson, "Resonant Raman scattering in cubic and hexagonal boron nitride," *Phys. Rev. B*, vol. 71, no. 20, p. 205201, May 2005.

29.   B. Arnaud, S. Lebègue, P. Rabiller, and M. Alouani, "Huge Excitonic Effects in Layered Hexagonal Boron Nitride," *Phys. Rev. Lett.*, vol. 96, no. 2, p. 026402, Jan. 2006.

30.   A. Bosak and M. Krisch, "Lattice dynamics of tetrahedrally bonded boron nitride probed by inelastic X-ray scattering," *Radiat. Phys. Chem.*, vol. 75, no. 11, pp. 1661–1665, Nov. 2006.

31.   B. Fakrach, A. Rahmani, H. Chadli, K. Sbai, and J. L. Sauvajol, "Raman spectrum of single-walled boron nitride nanotube," *Phys. E Low-dimensional Syst. Nanostructures*, vol. 41, no. 10, pp. 1800–1805, Oct. 2009.

32.   Q. Xu, V. R. Almeida, R. R. Panepucci, and M. Lipson, "Experimental demonstration of guiding and confining light in nanometer-size low-refractive-index material.," *Opt. Lett.*, vol. 29, no. 14, pp. 1626–8, Jul. 2004.

33.   R. Nemanich, S. Solin, and R. Martin, "Light scattering study of boron nitride microcrystals," *Phys. Rev. B*, vol. 23, no. 12, 1981.

34.   N. G. Chopra, R. J. Luyken, K. Cherrey, V. H. Crespi, M. L. Cohen, S. G. Louie, and A. Zettl, "Boron Nitride Nanotubes," *Science (80-.).*, vol. 269, no. 5226, pp. 966–967, 1995.

35.   L. Ci, L. Song, C. Jin, D. Jariwala, D. Wu, Y. Li, A. Srivastava, Z. F. Wang, K. Storr, L. Balicas, F. Liu, and P. M. Ajayan, "Atomic layers of hybridized boron nitride and graphene domains.," *Nat. Mater.*, vol. 9, no. 5, pp. 430–5, May 2010.

36.   O. Hod, "Graphite and Hexagonal Boron-Nitride Possess the Same Interlayer Distance. Why?," *J. Chem. Theory Comput.*, vol. 8, no. 4, pp. 1360–1369, 2012.

37.   D. Pacilé, J. C. Meyer, C. O. Girit, and a. Zettl, "The two-dimensional phase of boron nitride: Few-atomic-layer sheets and suspended membranes," *Appl. Phys. Lett.*, vol. 92, no. 13, p. 133107, 2008.

REPORT DOCUMENTATION PAGE

The public reporting burden for this collection of information is estimated to average 1 hour per response, including the time for reviewing instructions, searching existing data sources, gathering and maintaining the data needed, and completing and reviewing the collection of information. Send comments regarding this burden estimate or any other aspect of the collection of information, including suggestions for reducing this burden to Department of Defense, Washington Headquarters Services, Directorate for Information Operations and Reports (0704-0188), 1215 Jefferson Davis Highway, Suite 1204, Arlington, VA 22202-4302. Respondents should be aware that notwithstanding any other provision of law, no person shall be subject to an penalty for failing to comply with a collection of information if it does not display a currently valid OMB control number.
PLEASE DO NOT RETURN YOUR FORM TO THE ABOVE ADDRESS.

1. REPORT DATE *(DD-MM-YYYY)*	2. REPORT TYPE	3. DATES COVERED *(From – To)*
27-03-2014	Master's Thesis	Aug 2012 – Mar 2014

4. TITLE AND SUBTITLE

Structural Characterization of Atomically Thin Hexagonal Boron Nitride via Raman Spectroscopy

5a. CONTRACT NUMBER

5b. GRANT NUMBER

5c. PROGRAM ELEMENT NUMBER

6. AUTHOR(S)

Bondy, James, M, Capt, USAF

5d. PROJECT NUMBER

5e. TASK NUMBER

5f. WORK UNIT NUMBER

7. PERFORMING ORGANIZATION NAMES(S) AND ADDRESS(S)

Air Force Institute of Technology
Graduate School of Engineering and Management (AFIT/EN)
2950 Hobson Way
WPAFB OH 45433-7765

8. PERFORMING ORGANIZATION REPORT NUMBER

AFIT-ENP-14-M-02

9. SPONSORING/MONITORING AGENCY NAME(S) AND ADDRESS(ES)

Air Force Institute of Technology
Dr. Michael R. Snure
2241 Avionic Circle
Wright-Patterson AFB, OH 45433
michael.snure@us.af.mil

10. SPONSOR/MONITOR'S ACRONYM(S)

AFRL/RY

11. SPONSOR/MONITOR'S REPORT NUMBER(S)

N/A

12. DISTRIBUTION/AVAILABILITY STATEMENT

DISTRIBUTION STATEMENT A: APPROVED FOR PUBLIC RELEASE; DISTRIBUTION UNLIMITED.

13. SUPPLEMENTARY NOTES

This material is declared a work of the U.S. Government and is not subject to copyright protection in the United States.

14. ABSTRACT

A non-destruction evaluation of atomically thin hexagonal boron nitride (*h*-BN) films is critical to the U.S. Air Force and Department of Defense initiatives pursuing graphene-based electronic field effect transistors (FETs) capable of operating at terahertz frequencies. *H*-BN thin films an increase to the characteristic E_{2g} 1367cm^{-1} *h*-BN peak intensity has been correlated to an increase in film thickness. Raman spectroscopy on a *h*-BN film with thicknesses of 7, 14, and 21 atoms (2.5nm, 5nm, 7.5nm respectively) revealed a linear relationship between peak intensity and thickness. This relationship can mathematically be described as $y = 0.0265x + 0.8084$, and fits the data with a R^2 value of 0.9986. There was no observed correlation between film thickness and full width at half maximum (FWHM) and there was no measured shift to the E_{2g} peak with increasing film thickness.

15. SUBJECT TERMS

Hexagonal boron nitride; Raman spectroscopy; two-dimensional materials, nanotechnology

16. SECURITY CLASSIFICATION OF:			17. LIMITATION OF ABSTRACT	18. NUMBER OF PAGES	19a. NAME OF RESPONSIBLE PERSON
REPORT	**ABSTRACT**	**c. THIS PAGE**			Dr. Timothy W. C. Zens, AFIT/ENP
U	U	U	UU	71	**19b. TELEPHONE NUMBER** *(Include area code)* (937) 255-3636 x 4695 timothy.zens@afit.edu